

Modulation of chlorophyll concentration by downwelling Rossby waves during the winter monsoon in the southeastern Arabian Sea

P. Amol^{a,*}, Suchandan Bernal^b, D. Shankar^b, V. Jain^b, V. Thushara^c, V. Vijith^d, P. N. Vinayachandran^c

^aCSIR-National Institute of Oceanography, Regional Centre, Visakhapatnam, India

^bCSIR-National Institute of Oceanography, Goa, India

^cCentre for Atmospheric and Oceanic Sciences, Indian Institute of Science, Bengaluru, India

^dSchool of Marine Sciences, Cochin University of Science and Technology, Ernakulam, India

*Corresponding author *Email address:* amol@nio.org (P. Amol) *URL:* www.nio.org (P. Amol)

Abstract

Signatures of Rossby waves that are evident in satellite ocean colour data in the southeastern Arabian Sea (SEAS) are more prominent during the winter than the summer monsoon. During the winter, the sea level is high, and the conditions are less conducive for the injection of nutrients through the eddy-pumping mechanism. In this study, we use satellite observations and a physical-ecosystem model to examine the role of horizontal advection associated with Rossby waves in enhancing chlorophyll concentration in the SEAS. Zonal advection dominates over meridional advection, and its effect is more prominent in the south of Indian subcontinent and west of the Maldives. Except along the coast and around the islands, the vertical processes are weak and do not lead to a substantial increase in chlorophyll. Model simulations show that the currents associated with the Rossby wave also transport nutrients and other physicochemical properties of water along the path of the wave. The advected water decreases the concentration of Arabian Sea High Salinity water mass and replenishes the oxygen in the oxygen minimum zone in the SEAS.

Keywords: Rossby waves, Winter monsoon, Chlorophyll, Arabian Sea, Ecosystem modelling

1. Introduction

The Arabian Sea is known for intense winter blooms that occur because of the convective cooling that churns up the subsurface nutrients ([Banse & McClain, 1986](#); [Madhupratap et al., 1996](#); [Wiggert et al., 2000](#); [Lévy et al., 2007](#); [Shankar et al., 2016](#); [Vijith et al., 2016](#); [Keerthi et al., 2017](#)) (Figure 1). Owing to the strong bloom in the north, the dynamics of chlorophyll concentration in the southeastern Arabian Sea (SEAS) during the winter monsoon (November–February) has received less attention. Observations show that the downwelling that takes place along the eastern boundary of the Arabian Sea makes this region unfavourable for any blooms ([Banse, 1968](#); [Shankar et al., 2019](#)). The downwelling observed in this region owes its presence to the Kelvin waves that are generated by seasonal alongshore winds off the east coast of India and Sri Lanka ([McCreary et al., 1993](#); [Shankar & Shetye, 1997](#); [Suresh et al., 2016](#)). This downwelling wave propagates equatorward along the east coast and turns around Sri Lanka and propagates poleward along the west coast of India. As the wave propagates poleward, it spreads offshore as Rossby waves. The propagation of this wave leads to the formation of winter monsoon current (WMC) that bifurcates around the Rossby wavefront; one leg flows poleward and joins the West India Coastal Current (WICC), and the other leg continues to flow westward. As a consequence of these processes, the entire SEAS shows positive sea-level anomalies during the winter monsoon.

Observations from satellite ocean colour data show that the surface chlorophyll in the SEAS also drifts westward along with the Rossby waves ([Amol, 2018](#)). The westward drift is more prominent during the winter monsoon with the drift speed roughly matching the theoretical second baroclinic mode Rossby wave speed (Figure 1c,d). More recently, [Bemal et al. \(2019\)](#) showed that picoplankton community composition also changes across the Rossby front in the SEAS. The frontal region was dominated by phycoerythrin-rich *Synechococcus*, whereas the non-frontal regions had a higher abundance of phycocyanin-rich *Synechococcus* and *Prochlorococcus*.

Such link between surface chlorophyll and Rossby waves have been shown elsewhere ([Machu et al., 1999](#); [Cipollini et al., 2001](#); [Uz et al., 2001](#)), and several hypotheses have been proposed to explain this link. The hypotheses related to the vertical processes propose that the near-surface chlorophyll can increase either by upwelling ([Cipollini et al., 2001](#); [Uz et al., 2001](#)) or by shoaling of the subsurface chlorophyll maximum layer (SCML) ([Cipollini et al., 2001](#); [Kawamiya & Oschlies, 2001](#)). In the former case, the Rossby waves act as a ‘rototiller’ that pumps the nutrients into the mixed layer along the propagation path ([Siegel, 2001](#)). This mechanism has been observed near the Hawaiian Ocean Time Series station, where *in situ* observations show injections of cold nutrient-rich water into the euphotic zone during the passage of negative sea-level anomalies

(Sakamoto et al., 2004). Here, the elevated nitrate level leads to an increase in primary productivity and a shift in phytoplankton community structure. In the latter case, the shoaling makes the chlorophyll signal more visible to the satellite without any significant increase in productivity.

A more detailed study of satellite observations showed that the increase in chlorophyll is not always observed along the trough of the Rossby waves. Such an increase in chlorophyll is also observed along the convergence zone or the crest of the waves (Dandonneau et al., 2003; White et al., 2004; Killworth et al., 2004). Dandonneau et al. (2003) suggested that the increase in chlorophyll in the convergence zone was due to the accumulation of floating particulate organic carbon (fPOC). Here the Rossby waves act as “marine hay rakes”, which accumulates the floating particulates along the Rossby path. However, this process has not yet been validated using *in situ* observations, and its effectiveness is still contested (Killworth, 2004; Dandonneau et al., 2004).

A well-known hypothesis that explains this chlorophyll variability is the north-south advection against the mean background chlorophyll gradient (White et al., 2004; Killworth et al., 2004). In this mechanism, meridional currents associated with Rossby waves perturbs the mean north-south background gradient of the surface chlorophyll. Observations and modelling studies show that this process accounts for most of the observed chlorophyll variability associated with Rossby waves in the world ocean (Killworth et al., 2004; Charria et al., 2006; Gutknecht et al., 2010).

In the SEAS, the sea level is high during the winter, and the chlorophyll concentration is higher near the regions of strong currents (Amol, 2018). The eddy-pumping mechanism and the uplifting of SCML are associated with upwelling Rossby waves or negative sea-level anomalies and therefore cannot account for the increase in chlorophyll concentration in the SEAS. The unsteady nature of the basin and the closer proximity of the SEAS to the coast suggest that the north-south advection against the mean background gradient alone cannot explain the observed chlorophyll variability (Amol, 2018).

In this study, we identify the mechanisms that cause an increase in chlorophyll concentration in the SEAS during the winter monsoon using both observations and a physical ecosystem model. The details for the observations and the model are provided in the next section (Section 2). In Section 3, the role of horizontal advection in enhancing the chlorophyll concentration in the SEAS is shown using hydrography and satellite data. Then, the physical-ecosystem model is used to understand the impact of vertical processes (Section 4). The model is also used to highlight the effect of the westward drift of other biogeochemical variables in the SEAS. In the last section, we discuss and summarise the results (Section 5).

2. Data

2.1. Observations

Satellite data are used for model comparison and to highlight the importance of horizontal advection in modulating the chlorophyll concentration in the SEAS. The chlorophyll *a* climatology was from Sea-Viewing Wide Field-of-View Sensor (SeaWiFS) data, and the data can be downloaded from <http://oceancolor.gsfc.nasa.gov/SeaWiFS/>. The climatology for surface currents was computed from Ocean Surface Currents Analyses Real-time (OSCAR) data, which were available on a 0.33° grid for every five days. The data were provided by Physical Oceanography DAAC of the Jet Propulsion Laboratory and downloaded from <http://www.oscar.noaa.gov/>. The climatology for sea-level anomalies was from <http://www.aviso.altimetry.fr/en/data.html>. The values were computed relative to the mean from 1993 to 2018. (Hereon sea-level anomaly and chlorophyll *a* concentration are referred to as sea level and chlorophyll, respectively.)

Hydrographic observations from 08–15 November 2016 are used to show the vertical structure of chlorophyll in the SEAS across the Rossby wavefront. The east-west transect extended from (72.50°E, 9.50°N) to (75.34°E, 9.1°N) and had 19 stations (Figure 2). The stations were unequally spaced. At each station, the vertical profiles of temperature, salinity, and pressure were collected over top 500 m using a Sea-Bird 911Plus conductivity-temperature-depth (CTD) profiler. The profiler also contained auxiliary sensors that measured fluorescence and oxygen. The data from the CTD fluorescence sensor were validated using chlorophyll measurements from high-performance liquid chromatography (HPLC). The samples for the HPLC analysis were collected at selected depths (0, 5, 10, 15, 25, 50, 75, 100, and 150 m) for all stations. The linear regression analysis between the two data showed a positive relation with $R^2 = 0.629$ ($n = 278$, $P < 0.001$). The oxygen sensor (SBE 43) readings were also validated against the data obtained using the Winkler titration method on the water samples ($R^2 = 0.94$). The validation allows us to show the vertical distribution of chlorophyll and oxygen at a higher resolution. All the profiles were binned vertically at 1 m interval.

The current velocity data were obtained along the cruise track using a Teledyne RD Instruments (RDI) 150 kHz vessel-mounted acoustic Doppler current profiler (ADCP). The single ping data were collected at every eight-second interval and corrected for misalignment angle. Data were also screened based on RDI quality controlled model. Only horizontal velocities are shown here.

2.2. Model

A coupled physical-ecosystem model is used to analyse the chlorophyll variability in the SEAS. The model has been used to study the biophysical processes in the Arabian Sea ([Vijith et al., 2016](#); [Shankar et al., 2019](#)) and Bay of Bengal (BoB) ([Thushara & Vinayachandran, 2016](#); [Thushara et al., 2019](#); [Amol et al., 2019](#)). The model configuration used in this study is based on [Vijith et al. \(2016\)](#).

The model has two components: physical and ecosystem. The physical component is the Modular Ocean Model Version 4p1 ([Griffies et al., 2008](#)), and the model setup is similar to [Kurian & Vinayachandran \(2007\)](#). The horizontal resolution is 0.25° , and the vertical resolution varies from 5 m near the surface to 700 m at 5000 m depth. The domain extends from 30° E to 120° E and 30° S to 30° N. In the western and northern boundaries, a no-slip boundary condition is used, and there is no flux of heat or salt across the boundaries. For open boundaries, the temperature and salinity fields are relaxed to climatology ([Conkright et al., 1998](#)). The three-hour climatological forcing fields for atmospheric parameters like shortwave and longwave radiations, surface pressure, air temperature, and specific humidity are from European Centre for Medium-Range Weather Forecasts (ECMWF) Re-Analysis (ERA-Interim) ([Dee & Uppala, 2009](#)). The daily precipitation and climatological river runoff are from Tropical Rainfall Measuring Mission (TRMM) and Centre for Sustainability and the Global Environment (SAGE), respectively. The wind-speed and wind-stress forcings were created by merging daily winds from QuikSCAT with diurnal variability extracted from ERA-Interim ([Thushara & Vinayachandran, 2016](#)). The model produces a realistic representation of the seasonal cycle of temperature, salinity and currents in the Indian Ocean and has been used successfully to study the physical processes in the north Indian Ocean ([Kurian & Vinayachandran, 2007](#); [Vinayachandran et al., 2012](#); [Chatterjee et al., 2013](#); [Behara & Vinayachandran, 2016](#); [Shankar et al., 2016](#)).

The ecosystem component is the Tracers of Phytoplankton with Allometric Zooplankton (TOPAZ) model ([Dunne et al., 2010](#)) and has 25 tracers, which includes essential nutrients like nitrate, ammonium, phosphate, silicate, and iron. The biogeochemical cycle computation is based on flexible nutrient stoichiometry. The model accounts for nitrogen fixation, denitrification, atmospheric decomposition, gas exchange, scavenging, sediment processes, and river discharge. The model also includes dissolved organic matter and heterotrophic biomass. The three phytoplankton groups considered in the model are diazotrophs, small phytoplankton, and large phytoplankton. The phytoplankton physiology and growth is temperature-dependent ([Eppley, 1972](#)) and limited by light and nutrients ([Geider et al., 1998](#)). Nitrification is also light inhibited ([Ward et al., 1982](#)). Grazing is

parametrised based on size where at higher (lower) growth rates large (small) phytoplankton group dominates. The detritus production depends on both phytoplankton community composition and temperature. A detailed description of the model can be found in [Dunne et al. \(2010\)](#).

For model simulation, the physical model was started from a state of rest and was spun up for ten years using climatological temperature and salinity fields ([Conkright et al., 1998](#)). Following this spin-up, the physical model was coupled to the ecosystem model with initial conditions of nutrients obtained from the World Ocean Atlas (WOA09) ([Garcia et al., 2010](#)). The coupled model was integrated for another ten years. The results shown here are on the tenth year of the coupled-model spin-up.

3. Role of horizontal advection: hydrography and satellite

3.1. A transect across the Rossby front

In this section, we use hydrographic observations from a cruise during the winter monsoon of 2016 to highlight the influence of advection on the vertical structure of chlorophyll and other physicochemical variables (Figure 2). The vertical distribution of temperature, salinity, and oxygen (Figure: 3a,b,e) were already presented in [Bemal et al. \(2019\)](#), who used these measurements to show the impact of Rossby waves on the picoplankton community. We revisit these measurements to show the effect of Rossby waves on chlorophyll, water masses, and the oxygen minimum zone (OMZ) in the SEAS.

When the cruise began on 08 November, the sea level was high off the southwest coast of India (Figure 2). The first station of the west-east transect was sampled west of the zero sea level. As the cruise progressed, the high in sea level began to drift westward as a Rossby wave. By the time the last station was sampled (11 November), the zero contour had already crossed the first sampling station. The high in sea level initially forms off the southern tip of India during mid-October and drifts westward till December. The drift speed at 8.5°N is approximately 15 cm s⁻¹, which coincides with the second baroclinic Rossby wave speed observed in this region ([Shankar et al., 1996](#); [Amol, 2018](#)). The speed, however, increased to 17-19 cm s⁻¹ by mid-November, and this increase in speed is possibly due to the change in the stratification caused by the advection of the water mass with different physical properties. South of the Rossby wave is a strong cyclonic eddy at 7.5°N, which is quasi-stationary. Note that the observed Rossby wave is different from the annual Rossby wave seen in the climatology (Figure 1). From Figure 2, we can see that the annual Rossby wave is in its beginning stage with the signatures of WMC being evident at the southern tip of Sri Lanka.

As in [Bemal et al. \(2019\)](#), we have divided the transect into three regions: non-front west (NFW), front, and non-front east (NFE) (Figure 3). This division is based on the change in hydrographic properties along the transect. NFW consists of four stations west of 73°E, and NFE consists of four stations east of 74.8°E. The remaining stations are considered to be frontal stations. Here, we define front as a region characterised by large gradients in water properties like temperature, salinity or biogeochemical parameters ([Belkin et al., 2009](#); [Sarkar et al., 2018](#)). The front identified here is also associated with the Rossby wavefront around the zero sea-level contour and is linked to strong currents that are formed as a consequence of Rossby wave propagation.

Figure 3 shows that the near-surface properties of water in the frontal stations are distinctly different compared to those in the non-frontal stations. The mixed layer is thin, and the water is cooler and fresher at the front. This contrast in temperature and salinity is reflected in the density profile; the water is dense in the entire water column at the two non-front regions. Similarly, at the front, the oxycline is shallow, and the near-surface water has higher oxygen than the non-front. There are even differences between the two non-frontal stations. NFE is cooler and less salty compared to NFW, and the oxygen concentration is high at NFW at deeper depths. Below 50 m, there are signatures of downwelling; the isopycnals (and isothermals) are tilted downward from the front to NFW. Near the surface, the downwelling is overshadowed by a thin mixed layer containing low-salinity water. The downwelling signatures are also evident in the oxygen contours.

Within the 500 m water column depth, we identify two major water masses: the Arabian Sea High Salinity Water (ASHSW) and the Persian Gulf Water (PGW) ([Rochford, 1964](#)). ASHSW is characterised by high-saline water in the top 100 m. The density values range from 22.8–24.0 kg m⁻³. ASHSW forms during the winter monsoon in the northern Arabian Sea and spreads southward. The water mass is often detected near the surface, and it slides down under the fresher water that advects from BoB.

ASHSW is found between 25 and 75 m at the non-frontal stations and is more prominent at NFW (Figure 3b, 4). A thin layer of fresher water is present above ASHSW, and the layer is thicker at NFE compared to NFW. At frontal stations, ASHSW weakens and disappears for a few stations. Below ASHSW is the secondary maximum (SM) seen at NFE. This maximum is not evident at the front and NFW. The density of SM varies from 25.0–25.2 kg m⁻³. The density range is similar to the North Arabian Sea High Salinity Water (NASHSW), which is found north of 21°N in the central and eastern Arabian Sea ([Banse & Postel, 2009](#)). The water mass is also evident in the temperature-salinity (TS) diagrams shown in previous studies ([Kumar & Prasad, 1999](#); [Shankar](#)

et al., 2005; Shenoi et al., 2005). In Shankar et al. (2005) and Shenoi et al. (2005), the density of this SM was lower and ranged from 24.0–25.0 kg m⁻³. Shankar et al. (2005) consider this water mass as a part of ASHSW.

PGW, though present, is very weak at all stations (Figure 4). Following the analysis by Jain et al. (2017), we found small peaks of PGW in all three regions between 120 and 500 m (Figure not shown). The density range (26.2–26.8 kg m⁻³) of PGW lies between 120 and 375 m at NFW but at a deeper depth (220–400 m) at the front and NFE. They were almost absent in a few frontal and NFE stations (Stations 12, 16, 17). Unlike other physicochemical properties, there is no clear distinction in the magnitude of PGW between the frontal and non-frontal stations. One possible reason for this difference is the existence of PGW in the southern BoB (Jain et al., 2017). As the mixing is weak at these depth ranges, the PGW could be recirculated back to the SEAS from BoB because of the seasonal reversal in currents.

Like the water masses, the oxygen profiles in the three regions also show distinct differences. The low-oxygen layer (<0.5 mL L⁻¹) is at a shallower depth at NFW, extending from 70–190 m (Figure 3e). Below this layer, the water is well ventilated with the oxygen concentration going above 1 mL L⁻¹. At the front, this layer is seen between 210–270 m, and at NFE the layer is thicker and extends from 120–500 m.

The OMZ, which is typically characterised by <0.1 mL L⁻¹, is observed only at NFW between 90–120 m depth. The layer is evident above the PGW depth range. The slight increase in oxygen in the intermediate layers is sometimes associated with the advection of PGW (Law & Watson, 2001; Jain et al., 2017). The OMZ, in general, has an eastward shift in the basin and hugs the eastern boundary of the Arabian Sea (Naqvi, 1991; Banse et al., 2014). Observations from a recent study showed that the OMZ extended till ~ 10°N at 68°N during September–October 2016 (Shenoy et al., 2020). NFW stations are closer to this location, which implies that the southeastern boundary of OMZ could lie in the NFW region. It is also possible that OMZ existed at the front and NFE but was replaced with ventilated waters by the WMC.

The difference between the front and non-front is also evident in the vertical structure of the chlorophyll (Figure 3d). The non-front region has a deeper SCML, which lies between 30–60 m. The SCML in the front lies within the top 30 m and has a higher concentration of chlorophyll compared to non-frontal stations. Compared to NFW, the SCML at NFE is found at a shallower depth and is much thicker.

The ADCP currents are poleward in NFW and over the first few stations in the front (Figure 3f). The strongest current ($>50 \text{ cm s}^{-1}$) is observed on the western side of the frontal stations. The current extends till 100 m, with its core at around 50 m. In the eastern frontal stations, the current weakens, reverses, and flows south. This reversal is due to the formation of an eddy-like feature during 09-10 November (Figure 2). The current reverses again and flows poleward as seen in the last few stations of NFE. Comparison between the ADCP and OSCAR current shows that the ADCP current is stronger than OSCAR current west of 73.8°E (Figure 5a). In both the data sets, the current weakens farther east and then regains strength by the end of the cruise.

The strong currents, however, do not coincide with high chlorophyll values along the section (Figure 5b). Cross-correlation between the two data shows a time delay between the peak in the current and the peak in the surface chlorophyll; that is, the correlation between chlorophyll and current improves from -0.6 for a zero-day lag to 0.80 for a 12–14-day lag (Figure 5c). The analysis suggests that the chlorophyll takes time to respond to the changes in the magnitude of the current.

The observed lag and reversal in current also explain why the NFE is fresher and cooler than NFW. The strong poleward current carries the lighter water along the Rossby front. The front drifts westward, and the fresher water is replaced by saltier water from the north by a weak equatorward flow (Figure 3f). Because the replacement takes place over a shorter duration of time and by weaker currents, the water mass properties at NFE are identical to those at NFW but are less prominent.

3.2. Rossby wave in satellite-derived chlorophyll

The link between Rossby waves and surface chlorophyll in the SEAS was shown by [Amol \(2018\)](#) using two decades of unfiltered satellite data from the merged product the GlobColour. Though the Rossby wave signatures in sea level are evident during both winter monsoon and summer monsoon, the westward drift of chlorophyll is more prominent during the winter monsoon. This drift is also reflected in the monthly chlorophyll climatology (Figure 6a1–a4; also see [Amol \(2018\)](#) for details), with the chlorophyll signatures drifting more than 20 degrees westward. The high chlorophyll concentration ($> 0.2 \text{ mg m}^{-3}$) is evident east of Maldives during November, and it spreads westward from December to February. The chlorophyll begins to drop between the Maldives and Indian subcontinent from January to February even though the currents are strong. In order to isolate the mechanisms that lead to this enhancement of chlorophyll in the SEAS, we first compute the budget terms based on the advection equation using satellite data.

The advection equation for any tracer C can be written as

$$\overset{\text{Term 1}}{C_t} = -\overset{\text{Term 2}}{u}C_x - \overset{\text{Term 3}}{v}C_y - \overset{\text{Term 4}}{w}C_z + M. \quad (1)$$

Here, C represents the tracer (like chlorophyll or nitrate), and M includes the source and sink term; u , v , and w are the velocity components along the x , y , and z axes, respectively. Term 1 is the tendency term or the rate of change of tracer. Term 2, Term 3, and Term 4 are zonal, meridional, and vertical advection terms, respectively.

The tendency term shows that the chlorophyll decreases in November off the west coast of India and east of Maldives and increases elsewhere (Figure 7). This drop in the chlorophyll along the west coast during the winter monsoon is well known and is attributed to the poleward propagation of a seasonal downwelling Kelvin wave. The budget calculation using satellite data shows that meridional advection contributes to this decrease off the west coast of India, whereas zonal advection has an opposite effect.

During December, the chlorophyll increases over the region between the Maldives and Sri Lanka (Figure 6, 7a2). This increase is primarily due to zonal advection, which also plays a major role in enhancing the chlorophyll west of Maldives. The magnitude of meridional advection, though positive, is weaker compared to zonal advection.

The chlorophyll in the region between the Maldives and Sri Lanka drops during January and February, but the chlorophyll continues to increase west of Maldives (Figure 6, 7a3–a4). The zonal advection weakens east of Maldives and is still positive west of the Maldives with weaker contribution from meridional advection. In the central Arabian Sea, the chlorophyll begins to decrease by January. In short, the increase in chlorophyll owing to zonal advection is more evident south of the Indian subcontinent and west of the Maldives. The chlorophyll also decreases towards the west of Sri Lanka and increases again west of Maldives.

The above analysis does not, however, highlight the importance of vertical processes on the chlorophyll distribution. Previous studies (White et al., 2004; Killworth et al., 2004) have calculated the vertical advection term using a theoretical approximation based on the conservation of potential vorticity ($\beta v = fw_z$; where f is the Coriolis parameter, and β is the meridional gradient of Coriolis parameter). This approximation, which links the vertical velocity to meridional velocity, is more applicable to mid-latitude dynamics, in which the currents are in Sverdrup balance. The approximation would not hold in the north Indian Ocean because the basin is time-dependent at the lowest order. As no reliable observational data set is available in the SEAS to compute the vertical velocity terms, in the next section (Section 4), we use a numerical model to get its estimates.

3.3. The mean and perturbation terms

Studies from the other basins show that the most important term that explains the signature of Rossby waves on surface chlorophyll is the meridional advection term, which perturbs the mean background chlorophyll gradient (Killworth et al., 2004; Charria et al., 2006; Gutknecht et al., 2010). In order to identify the role of this mechanism, Killworth et al. (2004) used a simple model where they compared the amplitude ratio of the observed chlorophyll and sea level to the modelled terms. The observed amplitude ratio was obtained by identifying the frequency and wavelength of the peak in the cross-spectrum between chlorophyll and sea level. In the SEAS, though it is possible to resolve the dominant frequency, we cannot resolve the wavelength because of the small size of the basin. A typical first and second mode Rossby wavelength would range between 2000–5000 km at 12°N, which is comparable to the basin size. Nevertheless, we show that the simplifications made by Killworth et al. (2004) would not be sufficient to explain the processes in the SEAS because both the horizontal advection terms in Equation 1 would become important. The impact of each advection term would also vary from region to region.

We first decompose horizontal advection terms of Equation 1 into the sum of mean (C, u, v) and perturbation (C', u', v'). The advection terms can be rewritten as:

$$uC_x + vC_y = \overset{\text{Term 1}}{u'C_x} + \overset{\text{Term 2}}{uC'_x} + \overset{\text{Term 3}}{v'C_y} + \overset{\text{Term 4}}{vC'_y} \quad (2)$$

In the linearized model by Killworth et al. (2004), Term 1 and Term 4 in the RHS of Equation 2 are ignored. Term 3 represents the north-south advection against a mean background term. This term is known to account for most of the observed variability associated with Rossby waves. The east-west flow was assumed to be strong compared to the north-south flow (i.e. $v = u' = 0$) and therefore Term 2 is retained. This assumption holds because the five basins, which excludes the north Indian Ocean, have prominent zonal currents towards the north and south of the gyre and a relatively strong north-south chlorophyll gradient. The assumption would break down near the eastern and western boundary where the mean north-south flow could play an important role. Bonhomme et al. (2007), who had applied the conceptual model by Killworth et al. (2004), showed that Term 3 would still play an important role along the Peru coast, which lies at the eastern boundary of south Pacific Ocean. The Peru coast, however, is slanted between 5°S and 12°S, and its alignment would lead to a strong north-south chlorophyll gradient from the coast.

In Figure 8, we show the mean and standard deviation of both zonal and meridional velocities. The calculations show that the mean zonal velocity at the equator is eastward because of the presence of

strong Wyrski Jets during Autumn and Spring (Figure 8a1). The equatorial flow has a semi-annual period, and the flow reverses four times a year (Schott & McCreary, 2001; Shankar et al., 2002). The standard deviation of the equatorial currents is stronger towards the west of the basin. In the SEAS, the prominent flow is westward because the winter downwelling Rossby waves or the associated WMC is stronger compared to the summer upwelling Rossby waves (Shankar & Shetye, 1997). Higher standard deviation is also observed in this region. The Arabian Sea has a mean eastward flow compared to the Bay of Bengal. The mean flow, however, is much weaker compared to the standard deviation, which shows that the circulation in the north Indian Ocean is time-dependent at the lowest order (Figure 8c1). Unlike the north Indian Ocean, the south Indian Ocean is in a quasi-steady state, and the mean flow, owing to the westward flowing south equatorial current, is larger compared to the standard deviation.

In case of the meridional currents, the mean and the standard deviation is weaker compared to zonal currents except near the coast (Figure 8a2,b2). Also, the mean meridional flow is weaker compared to the fluctuations (Figure 8c2). The weak mean flow with strong standard deviation is also evident in direct current measurements along the coast of India (Amol et al., 2014; Mukherjee et al., 2014; Chaudhuri et al., 2020; Mukhopadhyay et al., 2020).

The mean and standard deviation of chlorophyll is stronger in the eastern Arabian Sea and along the coast of India (Figure 8a3,b3). In the eastern Arabian Sea, the mean and the fluctuating term have similar magnitudes, resulting in a weaker ratio (Figure 8c3). The standard deviation is much stronger in the SEAS, the eastern BoB, and the eastern equatorial Indian Ocean. However, in order to address the role of advection, the gradient of chlorophyll is more important compared to the mean and standard deviation.

Figure 9 shows that both horizontal and zonal gradients of chlorophyll are relatively weaker in the SEAS, but stronger in the western Arabian Sea, around the Maldives, and along the west coast of India. Around the Maldives, the zonal gradient is stronger compared to meridional. When averaged over the winter monsoon, the chlorophyll gradient still remains weak in the SEAS, but the mean current is strong owing to westward WMC (Figure not shown). In other words, the currents would dominate the chlorophyll gradient in the advection terms during the winter. In the rest of the basin, the chlorophyll gradient would play an important role.

The analysis shown here suggests that both zonal and meridional advection terms are important to explain the chlorophyll distribution in the north Indian Ocean. Unlike the Killworth et al. (2004) model, the Term 1 and Term 4 in Equation 2 cannot be neglected. The perturbed flow, whether zonal

or meridional, is more important in the open ocean, and the chlorophyll gradient is more important near the coast.

4. Rossby waves in coupled physical-ecosystem model

In this section, we begin by comparing the monthly climatology of surface chlorophyll during the winter monsoon (November–February) between the model and the observations (Figure 6). We show how various other model variables show a similar westward drift. The output from the numerical model is further used to highlight the role of vertical processes in enhancing the chlorophyll concentrations in the SEAS.

4.1. Westward drift: Impact of the Rossby waves on the ecosystem

Observations from the SEAS show that the low-salinity waters from BoB and temperature inversions that are formed due to air-sea fluxes drift westward along with the downwelling Rossby waves ([Shankar et al., 2004](#)). These processes are known to contribute to the formation of a huge warm pool in the Lakshadweep Sea, which peaks during May or early June ([Shenoi et al., 1999](#); [Rao & Sivakumar, 1999](#); [Kurian & Vinayachandran, 2007](#)). A similar impact of Rossby waves on chlorophyll concentration during the summer was envisaged by [Lévy et al. \(2007\)](#) based on a two-month lag seen in the onset of bloom between the region around India and the Lakshadweep Sea. However, the resolution of their numerical model limited their ability to resolve the wave propagation. Later, [Amol \(2018\)](#) confirmed this drift using satellite data for both summer and winter monsoon. In this section, we use a numerical model to show how various biogeochemical variables drift westward along with the Rossby wave. We discuss these results based on the available observations from the SEAS.

As in [Amol \(2018\)](#), we choose 0.2 mg m^{-3} contour to highlight the westward drift of chlorophyll associated with Rossby waves. Both the model and the observations show a westward drift in chlorophyll from November to February (Figure 6). During November, the 0.2 mg m^{-3} chlorophyll contour is restricted to the east of the Maldives Islands. However, the model chlorophyll is higher compared to the observation. By December, the 0.2 mg m^{-3} spreads west of the Maldives. The westward spreading is evident as a thin filament in the model compared to the observations. In the model, the chlorophyll is higher south of Sri Lanka and west of the Maldives. The chlorophyll weakens from Sri Lanka to the east of the Maldives. During January and February, the chlorophyll spreads farther west. Though the model chlorophyll is weaker compared to the observations during February, the westward drift is still evident in the model. The chlorophyll in the region between the Maldives and Indian subcontinent also weakens both in model and observations. In spite of the

differences between model and observations, the model is able to simulate the westward drift of the chlorophyll in the SEAS.

We now show how the westward drift impacts different phytoplankton groups in the SEAS. The model decomposes the phytoplankton into three groups: small phytoplankton, large phytoplankton, and diazotrophs. The simulation shows that the small phytoplankton group dominates the SEAS during the entire winter monsoon (Figure 6). Hence, the westward drift is more evident in the small phytoplankton group compared to the other two phytoplankton groups in the SEAS. The small phytoplankton group in the model represent the picoplankton/nanoplankton community loosely characterised as cyanobacteria (Dunne et al., 2010), and they play an important role in the microbial loop. The observations of Bernal et al. (2019) support the model results and show how the Rossby waves modify the picoplankton community structure in the SEAS. In their study, the advected low-salinity water, which is associated with the Rossby wave front, contains a higher concentration of phycoerythrin-rich *Synechococcus*, particularly in the mixed layer. The picoplankton constitutes more than 83% of the total chlorophyll, and they were not very evident at non-front stations where picoplankton groups like *Prochlorococcus* and phycocyanin-rich *Synechococcus* dominated the water column. At the non-front stations, the picoplankton contribution to the total chlorophyll dropped to less than 50%. This drop is not evident in the model as the small phytoplankton is the dominant group in the deeper waters.

The nitrate distribution is similar to that of the chlorophyll (Figure 10a1–a4). The nitrate spreads westward from November to February, but the spreading is very weak for ammonium. Compared to nitrate, a higher concentration of ammonium is present west of the Maldives and off the west coast of India during November. Except over the regions where the nitrate drifts westward and the coastal regimes, the ammonium is slightly higher in the SEAS during the entire winter monsoon. Earlier observations from this region have shown higher concentration of nitrate in the SEAS compared to the central west coast of India (Kumar et al., 2004; Rao et al., 2017). The higher nitrate coincided with lower salinity and elevated surface chlorophyll. Both phosphate and silicate also show a similar westward drift particularly south of Sri Lanka and west of the Maldives (Figure 10c1–c4, d1–d4). During November, the phosphate is higher off the southwest coast of India. As the season progresses, lower phosphate appears to spread poleward along with the poleward WICC. By February, low phosphate is observed in the entire SEAS. This intrusion of low phosphate from the south is evident in the observations of Bernal et al. (2019). The near-surface phosphate levels were found lower in the regions of strong currents, but on either side of the strong currents, the phosphates were higher, with the largest concentration observed near the coast. Unlike the other variables, the silicate continues to

increase in the region between the Maldives and Sri Lanka till February because of strong currents. The presence of silicate indicates the presence of low-salinity water of riverine origin. The higher concentration of silicate in the SEAS is also evident in observations ([Rao et al., 2017](#)) and simulations by [Young & Kindle \(1994\)](#).

Though the nutrient observations are sparse in this region, the available data hinted on the effect of Rossby waves on nutrient dynamics in the SEAS.

4.2. Role of vertical processes

In this section, we compute the horizontal and vertical advection budget terms (Equation [1](#)) using the model chlorophyll. As chlorophyll is a diagnostic variable in the model, we do not separate the two mechanisms – the upliftment of subsurface chlorophyll maximum layer and the injection of nutrients from the subsurface waters – that lead to enhancement of chlorophyll by Rossby waves.

The budget analysis shows that the tendency and the horizontal advection terms from the model match the observations, but there are differences in the magnitude (Figure [11](#)). As seen in the observations, the zonal advection primarily contributes to the increase in chlorophyll south of India and west of the Maldives. The magnitude of the meridional advection term is weaker compared to that of the zonal advection term in these two regions (Figure [12](#)). These are the regions where the westward drift owing to the Rossby wave propagation is evident in the chlorophyll climatology (Figure [6](#)). The meridional advection is stronger towards the northwest of the Maldives, and this region extends till the west coast of India (Figure [12](#)). The region is slanted from southwest to northeast and roughly aligns with the Rossby wavefront. The Rossby wavefront, which represents the region around the zero-contour of sea level, is associated with relatively stronger meridional currents. The role of the meridional current is also evident in the hydrography data shown in Section [3.1](#).

The vertical advection term is in general weaker compared to the horizontal advection terms (Figure [11,12](#)). The advection term weakens along the coast of India from December because of the poleward propagating downwelling Kelvin wave ([Shankar & Shetye, 1997](#)). Patches of strong vertical advection are observed near the coast and around the Maldives, but this term does not play an important role in the regions where the westward drift of chlorophyll is prominent (Figure [11](#)). The magnitude of vertical advection is stronger compared to horizontal advection north of the Maldives during January and February and southwest of the Maldives during December and February (Figure [12](#)).

Though the analysis shows the dominance of horizontal advection, the question pertaining to the supply of nutrients required for the sustenance of phytoplankton in the SEAS still remains. In order to answer this question, we picked two regions where the nitrate is high; one is the southern coast of Sri Lanka, and the other is the Maldives (Figure 13). We identify these two regions as source points from where the nutrients are supplied to the rest of the SEAS.

The nitrate budget shows that the vertical processes peak between November and January around the southeast coast of Sri Lanka (Figure 13c). The nutrients supplied by the vertical processes are then advected by the currents into the SEAS (Figure 13b). As the vertical processes weaken after January, the role of horizontal advection becomes less significant even though the currents are reasonably strong. The chlorophyll decreases between the Maldives and Indian subcontinent during February because of the weak supply of nutrients from the subsurface waters, whereas the silicate keeps on increasing because of strong currents (Figure 6, 10). A similar scenario is evident in the region around Maldives (Figure 13d–f). The vertical terms are higher in the region between the islands during the winter monsoon, and the nutrients supplied by the vertical processes are carried farther eastward by zonal advection.

5. Discussion

The enhancement of chlorophyll concentration in the SEAS is analogous to the bloom observed in the southwestern BoB during the summer monsoon (Vinayachandran et al., 2004; Lévy et al., 2007). The bloom is formed due to the advection of upwelled water from the coast of Sri Lanka to the BoB by the summer monsoon current (SMC). Similarly, the WMC carries the nutrient-rich waters from the region around the Sri Lanka coast and the Maldives and enhances the chlorophyll in the entire the SEAS. Though the advected chlorophyll is weaker compared to that caused by summer monsoon current, the presence of the Maldives along the Rossby wave path allows the wave signatures in chlorophyll to extend farther west.

In addition to the advection of water, the depth of SCML would also play an essential role in the chlorophyll distribution in the SEAS. The nearness of the SCML to the surface would affect the amount of chlorophyll detected by the satellite. The hydrographic profiles show that the SCML lies in the top 30 m across the Rossby front, and this depth is well within the penetration range of the satellite. Earlier studies have linked the shoaling of SCML to the upwelling Rossby waves, which tilts the isopycnals upwards along the wavepath (Cipollini et al., 2001; Kawamiya & Oschlies, 2001). In the SEAS, the currents associated with Rossby wave transport water containing a shallow SCML with higher chlorophyll concentration.

Both observations (Bemal et al., 2019) and the model simulation show a higher concentration of small phytoplankton in the advected waters. The dominance of small phytoplankton would make sense because the phytoplankton is less dependent on the amount of nutrient available in the water (Chisholm, 1992; Kjørboe, 1993; Raven, 1998; Bemal et al., 2018). Compared to large phytoplankton, the small phytoplankton would sustain for longer duration as the water is advected over a larger distance from the source. The scenario is different during the summer monsoon when the near-coastal chlorophyll is dominated by large phytoplankton (Shankar et al., 2019). The large phytoplankton owes its presence to the strong upwelling that takes place along the southwest coast of India. Shankar et al. (2019) suggested that the size of the phytoplankton has implications for the nature of fisheries in the eastern Arabian Sea. The presence of large phytoplankton generally leads to a smaller food chain in the SEAS because the phytoplankton can be directly fed on by planktivorous fishes. The smaller group introduced by Rossby waves would change the phytoplankton composition and possibly have an impact on the higher trophic levels in this region.

The reason for the availability of nutrients and the presence of phytoplankton off the southeast coast of Sri Lanka and the region around the Maldives needs to be further investigated. For example, the high chlorophyll around the Maldives could be generated by several fine-scale processes like island stirring by currents, local upwelling, or generation of cyclonic eddies that could pump up the nutrients. The enhancement of chlorophyll, often referred to as ‘island mass effect’, varies greatly among the different channels of the Maldives islands (Sasamal, 2006). Though our model simulation highlights the importance of vertical processes in these regions, *in situ* observations along with a high-resolution regional model would be needed to resolve these fine-scale processes. Similarly, de Vos et al. (2014) suggested that the convergence of coastal currents could lead to upwelling along the southern coast of Sri Lanka. The upwelling in their model was observed off the southwest coast of Sri Lanka and was weaker. In another study, Luis & Kawamura (2000) used satellite data to show that the winds that blow in the gap between India and Sri Lanka could lower the SST in the SEAS by entrainment mixing. This wind-driven mixing, which decreases the SST, has the potential to pump up nutrients and enhance productivity. The high chlorophyll could also be due to the presence of river nutrients in the low-salinity water advected by the currents, but the absence of river nutrients in our model simulation suggests otherwise. Without the river nutrients, the model captures the westward drift and highlights the importance of vertical process along the southeastern coast of Sri Lanka.

The region around the southern coast of Sri Lanka is also well known for blue whale sightings (*Balaenoptera musculus*), particularly during winter monsoon (Charles et al., 2012). A similar peak in sightings during the winter is also evident in the region around the Maldives. The presence of

these large organisms suggests an active ecosystem with large productive feeding ground, which implies that these two regions can act as a source for the supply of the nutrients to the rest of the SEAS. The loss of nutrients by horizontal advection would also impact the ecosystem in these two regions, with the vertical supply of nutrients weakening after the winter monsoon.

Climate modes, like Indian Ocean Dipole (IOD) and El Niño/Southern Oscillation (ENSO), are known to be important drivers of interannual variability of chlorophyll concentration in the Arabian Sea (Wiggert et al., 2002; Sarma, 2006; Jayaram et al., 2013; Currie et al., 2013; Keerthi et al., 2017). The hydrography measurements shown in this study took place during a negative IOD year, which was one of the strongest in the past two decades (Lu et al., 2018). Anomalously strong blooms are also evident in ocean colour data in the SEAS during the summer monsoon, and this increase in chlorophyll was attributed to two cold-core eddies formed in the SEAS and IOD by Thushara & Vinayachandran (2020). The bloom decayed by the end of October. The study by Currie et al. (2013) showed that the IOD has a negative influence on chlorophyll concentrations in the region around Sri Lanka during the winter. When combined with ENSO, the impact of the climate modes on surface chlorophyll improves, but ENSO on its own has a very weak effect on the chlorophyll variability. Though satellite ocean colour data show strong interannual variability in the westward drift of chlorophyll in the SEAS (see Figure S2, supplemental material in Amol, 2018), a detailed analysis would be required to delineate the processes pertaining to this variability.

The prominent role of ocean currents on the spatial distribution of OMZ in the Arabian Sea has been noted earlier (Swallow, 1984; Sarma, 2002; Resplandy et al., 2012; McCreary et al., 2013). Model simulations by McCreary et al. (2013) show that the OMZ would expand toward the south in the absence of horizontal advection, and the currents south of 12°N play a dominant role in limiting this expansion. The oxygen variability in the SEAS has also been linked to Rossby and coastal Kelvin waves (Resplandy et al., 2012; Shenoy et al., 2020). The study by Resplandy et al. (2012) shows that the undercurrents below 200 m transport low-oxygen water southwards along the west coast of India during the winter monsoon. In our data, the OMZ is at a shallower depth (90–120 m), and no reversal in current is seen till 200 m (Figure 3e,f). The observation highlights the role of near-surface currents in modulating the low-oxygen waters.

The westward propagation of Rossby waves also would also have an impact on the distribution of water masses in the southern Arabian Sea. These water masses travel over vast distances, including BoB (Rochford, 1964), and the currents associated with the Rossby wave could play an important role in their seasonal distribution. The change in water mass properties would take place gradually from east to west because of the direction of the Rossby wave propagation.

In summary, the calculation of budget terms shows that the zonal advection plays a major role in the enhancement of chlorophyll in the SEAS, particularly where the westward WMC is strong. Meridional advection also contributes along the Rossby front, but it has an opposite effect closer to the west coast of India. Around the coast of Sri Lanka and Maldives, both the horizontal and the vertical processes enhance the chlorophyll. The vertical processes, however, weaken farther west of the Maldives and Sri Lanka. The islands in the Maldives play an essential role in replenishing the chlorophyll along the Rossby path, owing to which signatures of the Rossby wave are present even westward of 60°E.

6. Acknowledgments

This work is part of TRIMFish, a project funded by the Council of Scientific and Industrial Research (CSIR), India. Model simulations were carried out on Mandhan supercomputer at Centre for Atmospheric and Oceanic Sciences and on SahasraT (CrayXC40) at Supercomputer Education and Research Centre, Indian Institute of Science (IISc). The Mandhan supercomputer was funded by the Fund for Improvement of S&T Infrastructure (FIST), DST, and Divecha Centre for Climate Change, IISc. We would like to acknowledge Dr M. S. Krishna, ship officers, crew, and colleagues for providing us with the necessary support in collecting data. We also thank Dr A. C. Anil and Dr S. G. Aparna for their critical comments. This is NIO Contribution XXXX.

References

- Amol, P. (2018). Impact of Rossby waves on chlorophyll variability in the southeastern Arabian Sea. *Remote Sensing Letters*, 9, 1214–1223. doi:[10.1080/2150704X.2018.1504335](https://doi.org/10.1080/2150704X.2018.1504335).
- Amol, P., Shankar, D., Fernando, V., Mukherjee, A., Aparna, S., Fernandes, R., Michael, G., Khalap, S., Satelkar, N., Agarvadekar, Y., Gaonkar, M., Tari, A., Kankonkar, A., & Vernekar, S. (2014). Observed intraseasonal and seasonal variability of the West India Coastal Current on the continental slope. *Journal of Earth System Science*, 123, 1045–1074. doi:[10.1007/s12040-014-0449-5](https://doi.org/10.1007/s12040-014-0449-5).
- Amol, P., Vinayachandran, P. N., Shankar, D., Thushara, V., Vijith, V., Chatterjee, A., & Kankonkar, A. (2019). Effect of freshwater advection and winds on the vertical structure of chlorophyll in the northern Bay of Bengal. *Deep Sea Research Part II*, . doi:[10.1016/j.dsr2.2019.07.010](https://doi.org/10.1016/j.dsr2.2019.07.010).
- Banse, K. (1968). Hydrography of the Arabian Sea Shelf of India and Pakistan and effects on demersal fishes. *Deep Sea Research and Oceanographic Abstracts*, 15, 45 – 79. doi:[10.1016/0011-7471\(68\)90028-4](https://doi.org/10.1016/0011-7471(68)90028-4).
- Banse, K., & McClain, C. R. (1986). Winter blooms of phytoplankton in the Arabian Sea as observed by Coastal Zone Color Scanner. *Mar. Ecol. Prog. Ser.*, 34, 201–211.
- Banse, K., Naqvi, S. W. A., Narvekar, P. V., Postel, J. R., & Jayakumar, D. A. (2014). Oxygen minimum zone of the open Arabian Sea: variability of oxygen and nitrite from daily to decadal timescales. *Biogeosciences*, 11, 2237–2261. doi:[10.5194/bg-11-2237-2014](https://doi.org/10.5194/bg-11-2237-2014).
- Banse, K., & Postel, J. R. (2009). Wintertime convection and ventilation of the upper pycnocline in the northernmost Arabian Sea. *Geophysical Monograph Series*, 185, 87–117. doi:[10.1029/2008GM000704](https://doi.org/10.1029/2008GM000704).
- Behara, A., & Vinayachandran, P. N. (2016). An OGCM study of the impact of rain and river water forcing on the Bay of Bengal. *Journal of Geophysical Research*, 121, 2425–2446. doi:[10.1002/2015JC011325](https://doi.org/10.1002/2015JC011325).
- Belkin, I. M., Cornillon, P. C., & Sherman, K. (2009). Fronts in Large Marine Ecosystems. *Progress in Oceanography*, 81, 223–236. doi:[10.1016/j.pocean.2009.04.015](https://doi.org/10.1016/j.pocean.2009.04.015). Comparative Marine Ecosystem Structure and Function: Descriptors and Characteristics.
- Bemal, S., Anil, A. C., & Amol, P. (2019). Picophytoplankton variability: Influence of Rossby wave propagation in the southeastern Arabian Sea. *Journal of Marine Systems*, 199. doi:[10.1016/j.jmarsys.2019.103221](https://doi.org/10.1016/j.jmarsys.2019.103221).
- Bemal, S., Anil, A. C., Shankar, D., Remya, R., & Roy, R. (2018). Picophytoplankton variability: Influence of winter convective mixing and advection in the northeastern Arabian Sea. *Journal of Marine Systems*, 180, 37–48. doi:[10.1016/j.jmarsys.2017.12.007](https://doi.org/10.1016/j.jmarsys.2017.12.007).
- Bonhomme, C., Aumont, O., & Echevin, V. (2007). Advective transport caused by intraseasonal Rossby waves: A key player of the high chlorophyll variability off the Peru upwelling region. *Journal of Geophysical Research: Oceans*, 112. doi:[10.1029/2006JC004022](https://doi.org/10.1029/2006JC004022).

Charles, A., Branch, T., Alagiyawadu, A., Baldwin, R., & Marsac, F. (2012). Seasonal distribution, movements and taxonomic status of blue whales (*Balaenoptera musculus*) in the northern Indian Ocean. *Journal of Cetacean Resources and Management*, *12*, 203–218.

Charria, G., Dadou, I., Cipollini, P., Drévilion, M., Mey, P. D., & Garçon, V. (2006). Understanding the influence of Rossby waves on surface chlorophyll *a* concentrations in the North Atlantic Ocean. *Journal of Marine Research*, *64*, 43–71. doi:[10.1357/002224006776412340](https://doi.org/10.1357/002224006776412340).

Chatterjee, A., Shankar, D., McCreary, J. P., & Vinayachandran, P. N. (2013). Yanai waves in the western equatorial Indian Ocean. *Journal of Geophysical Research*, *118*, 1556–1570. doi:[10.1002/jgrc.20121](https://doi.org/10.1002/jgrc.20121).

Chaudhuri, A., Shankar, D., Aparna, S. G., Amol, P., Fernando, V., Kankonkar, A., Michael, G. S., Satelkar, N. P., Khalap, S. T., Tari, A. P., Gaonkar, M. G., Ghatkar, S., & Khedekar, R. R. (2020). Observed variability of the West India Coastal Current on the continental slope from 2009–2018. *Journal of Earth System Science*, *129*, 57. doi:[10.1007/s12040-019-1322-3](https://doi.org/10.1007/s12040-019-1322-3).

Chisholm, S. (1992). Phytoplankton size. In F. P.G., W. A.D., & V. K. (Eds.), *Primary productivity and biogeochemical cycles in the sea* (pp. 213–237). Springer, Boston, MA volume 43 of *Environmental Science Research*.

Cipollini, P., Cromwell, D., Challenor, P. G., & Raffaglio, S. (2001). Rossby waves detected in global ocean colour data. *Geophysical Research Letters*, *28*, 323326. doi:[10.1029/1999GL011231](https://doi.org/10.1029/1999GL011231).

Conkright, M. E., Levitus, S., O'Brien, T., Boyer, T. P., Antonov, J. J., & Stephens, C. (1998). *World Ocean Atlas 1998 [CD-ROM]*, NODC Int. Rep. 15. Technical Report NOAA, Silver Spring, Md.

Currie, J. C., Lengaigne, M., Vialard, J., Kaplan, D. M., Aumont, O., Naqvi, S. W. A., & Maury, O. (2013). Indian Ocean Dipole and El Niño Southern Oscillation impacts on regional chlorophyll anomalies in the Indian Ocean. *Biogeosciences*, *10*, 6677–6698. doi:[10.5194/bg-10-6677-2013](https://doi.org/10.5194/bg-10-6677-2013).

Dandonneau, Y., Menkes, C., Gorgues, T., & Madec, G. (2004). “Response to comment on Oceanic Rossby waves acting as a ‘hay rake’ for ecosystem floating by-products”. *Science*, *304*.

Dandonneau, Y., Vega, A., Loisel, H., Du Penhoat, Y., & Menkes, C. (2003). Oceanic Rossby waves acting as a “hay rake” for ecosystem floating by-products. *Science*, *302*, 1548–1551.

Dee, D. P., & Uppala, S. (2009). Variational bias correction of satellite radiance data in the ERA-Interim reanalysis. *Quarterly Journal of the Royal Meteorological Society*, *135*, 1830–1841. doi:[10.1002/qj.493](https://doi.org/10.1002/qj.493).

Dunne, J. P., Gnanadesikan, A., Sarmiento, J. L., & Slater, R. D. (2010). Technical description of the prototype version (v0) of tracers of phytoplankton with allometric zooplankton (TOPAZ) ocean bio-geochemical model as used in the Princeton IFMIP model. *Biogeosciences*, *3593*.

Eppley, R. W. (1972). Temperature and phytoplankton growth in the sea. *Fishery Bulletin*, *70*, 1063–1085.

Garcia, H. E., Locarnini, R. A., Boyer, T. P., Antonov, J. I., Zweng, M. M., Baranova, O. K., & Johnson, D. R. (2010). Nutrients (Phosphate, Nitrate, Silicate). U.S. Gov. Print. Off., Washington, D. C. volume 4 of *World Ocean Atlas 2009*.

Geider, R. J., MacIntyre, H. L., & Kana, T. M. (1998). A dynamic regulatory model of phytoplankton acclimation to light, nutrients, and temperature. *Limnology and Oceanography*, *43*, 679–694. doi:[10.4319/lo.1998.43.4.0679](https://doi.org/10.4319/lo.1998.43.4.0679).

Griffies, S. M., Harrison, M. J., Pacanowski, R. C., & Rosati, A. (2008). *A technical guide to MOM4*, GFDL Ocean Group. Technical Report 5 Fluid Dyn. Lab., NOAA, Princeton.

Gutknecht, E., Dadou, I., Charria, G., Cipollini, P., & Garçon, V. (2010). Spatial and temporal variability of the remotely sensed chlorophyll a signal associated with Rossby waves in the South Atlantic Ocean. *Journal of Geophysical Research*, *115*. doi:[10.1029/2009JC005291](https://doi.org/10.1029/2009JC005291).

Jain, V., Shankar, D., Vinayachandran, P. N., Kankonkar, A., Chatterjee, A., Amol, P., Almeida, A. M., Michael, G. S., Mukherjee, A., Chatterjee, M., Fernandes, R., Luis, R., Kamble, A., Hegde, A. K., Chatterjee, S., Das, U., & Neema, C. P. (2017). Evidence for the existence of Persian Gulf Water and Red Sea Water in the Bay of Bengal. *Climate Dynamics*, *48*, 3207–3226. doi:[10.1007/s00382-016-3259-4](https://doi.org/10.1007/s00382-016-3259-4).

Jayaram, C., Kochuparambil, A. J., & Balchand, A. N. (2013). Interannual variability of chlorophyll *a* concentration along the southwest coast of India. *International Journal of Remote Sensing*, *34*, 3820–3831. doi:[10.1080/01431161.2012.762482](https://doi.org/10.1080/01431161.2012.762482).

Kawamiya, M., & Oschlies, A. (2001). Formation of a basin-scale surface chlorophyll pattern by Rossby waves. *Geophysical Research Letters*, *28*, 4139–4142.

Keerthi, M. G., Lengaigne, M., Levy, M., Vialard, J., Parvathi, V., de Boyer Montégut, C., Ethé, C., Aumont, O., Suresh, I., Akhil, V. P., & Muraleedharan, P. M. (2017). Physical control of interannual variations of the winter chlorophyll bloom in the northern Arabian Sea. *Biogeosciences*, *14*, 3615–3632. doi:[10.5194/bg-14-3615-2017](https://doi.org/10.5194/bg-14-3615-2017).

Killworth, P. D. (2004). Comment on “Oceanic Rossby waves acting as a ‘Hay Rake’ for ecosystem floating by-products”. *Science*, *304*. doi:[10.1126/science.1094870](https://doi.org/10.1126/science.1094870).

Killworth, P. D., Cipollini, P., Uz, B. M., & Blundell, J. R. (2004). Physical and biological mechanisms for planetary waves observed in sea-surface chlorophyll. *Journal of Geophysical Research*, *109*. doi:[10.1029/2003JC001768](https://doi.org/10.1029/2003JC001768).

Kjørboe, T. (1993). Turbulence, phytoplankton cell size, and the structure of pelagic food webs. (pp. 1–72). Academic Press volume 29 of *Advances in Marine Biology*. doi:[10.1016/S0065-2881\(08\)60129-7](https://doi.org/10.1016/S0065-2881(08)60129-7).

Kumar, S. P., Narvekar, J., Kumar, A., Shaji, C., Anand, P., Sabu, P., Rijomon, G., Josia, J., Jayaraj, K. A., Radhika, A., & Nair, K. K. C. (2004). Intrusion of the Bay of Bengal water into the Arabian Sea during winter monsoon and associated chemical and biological response. *Geophysical Research Letters*, *31*, L15304. doi:[10.1029/2004GL020247](https://doi.org/10.1029/2004GL020247).

Kumar, S. P., & Prasad, T. G. (1999). Formation and spreading of Arabian Sea high-salinity water mass. *Journal of Geophysical Research: Oceans*, *104*, 1455–1464. doi:[10.1029/1998JC900022](https://doi.org/10.1029/1998JC900022).

Kurian, J., & Vinayachandran, P. N. (2007). Mechanisms of formation of the Arabian Sea mini warm pool in a high-resolution Ocean General Circulation Model. *Journal of Geophysical Research: Oceans*, *112*. doi:[10.1029/2006JC003631](https://doi.org/10.1029/2006JC003631). C05009.

Law, C. S., & Watson, A. J. (2001). Determination of Persian Gulf Water Transport and oxygen utilisation rates using SF₆ as a novel transient tracer. *Geophysical Research Letters*, *28*, 815–818. doi:[10.1029/1999GL011317](https://doi.org/10.1029/1999GL011317).

Lévy, M., Shankar, D., André, J. M., Shenoi, S. S. C., Durand, F., & de Boyer Montégut, C. (2007). Basin-wide seasonal evolution of the Indian Ocean's phytoplankton blooms. *Journal of Geophysical Research: Oceans*, *112*. doi:[10.1029/2007JC004090](https://doi.org/10.1029/2007JC004090).

Lu, B., Ren, H.-L., Scaife, A. A., Wu, J., Dunstone, N., Smith, D., Wan, J., Eade, R., MacLachlan, C., & Gordon, M. (2018). An extreme negative Indian Ocean Dipole event in 2016: dynamics and predictability. *Climate Dynamics*, *51*, 89–100. URL: [10.1007/s00382-017-3908-2](https://doi.org/10.1007/s00382-017-3908-2).

Luis, A. J., & Kawamura, H. (2000). Wintertime Wind Forcing and Sea Surface Cooling Near the South India Tip Observed Using NSCAT and AVHRR. *Remote Sensing of Environment*, *73*, 55–64. doi:[10.1016/S0034-4257\(00\)00081-X](https://doi.org/10.1016/S0034-4257(00)00081-X).

Machu, E., Ferret, B., & Garçon, V. (1999). Phytoplankton pigment distribution from SeaWiFS data in the subtropical convergence zone south of Africa: a wavelet analysis. *Geophysical Research Letters*, *26*, 1469–1472.

Madhupratap, M., Kumar, S. P., Bhattathiri, P. M. A., Kumar, M. D., Raghukumar, S., Nair, K. K. C., & Ramaiah, N. (1996). Mechanism of the biological response to winter cooling in the northeastern Arabian Sea. *Nature*, *384*, 549–552. doi:[10.1038/384549a0](https://doi.org/10.1038/384549a0).

McCreary, J. P., Kundu, P. K., & Molinari, R. L. (1993). A numerical investigation of dynamics, thermodynamics and mixed-layer processes in the Indian Ocean. *Progress in Oceanography*, *31*, 181–244. doi:[10.1016/0079-6611\(93\)90002-U](https://doi.org/10.1016/0079-6611(93)90002-U).

McCreary, J. P., Yu, Z., Hood, R. R., Vinayachandran, P., Furue, R., Ishida, A., & Richards, K. J. (2013). Dynamics of the Indian-Ocean oxygen minimum zones. *Progress in Oceanography*, *112–113*, 15–37. doi:[10.1016/j.pocean.2013.03.002](https://doi.org/10.1016/j.pocean.2013.03.002).

Mukherjee, A., Shankar, D., Fernando, V., Amol, P., Aparna, S., Fernandes, R., Michael, G., Khalap, S., Satelkar, N., Agarvadekar, Y., Gaonkar, M., Tari, A., Kankonkar, A., & Vernekar, S. (2014). Observed seasonal and intraseasonal variability of the East India Coastal Current on the continental slope. *Journal of Earth System Science*, *123*, 1197–1232. doi:[10.1007/s12040-014-0471-7](https://doi.org/10.1007/s12040-014-0471-7).

Mukhopadhyay, S., Shankar, D., Aparna, S. G., Mukherjee, A., Fernando, V., Kankonkar, A., Khalap, S. T., Satelkar, N. P., Gaonkar, M. G., Tari, A. P., Khedekar, R. R., & Ghatkar, S. (2020). Observed variability of the East India Coastal Current on the continental slope during 2009–2018. doi:doi.org/10.1007/s12040-020-1346-8 accepted.

Naqvi, S. (1991). Geographical extent of denitrification in the Arabian Sea in relation to some physical processes. *Oceanologica Acta*, *14*, 281–290.

Rao, G. D., Kanuri, V. V., Kumaraswami, M., Ezhilarasan, P., Rao, V., Patra, S., Dash, S., Peter, M., Rao, V. R., & Ramu, K. (2017). Dissolved nutrient dynamics along the southwest coastal waters of India during northeast monsoon: a case study. *Chemistry and Ecology*, *33*, 229–246. doi:[10.1080/02757540.2017.1287903](https://doi.org/10.1080/02757540.2017.1287903).

Rao, R. R., & Sivakumar, R. (1999). On the possible mechanisms of the evolution of a mini-warm pool during the pre-summer monsoon season and the genesis of onset vortex in the South-Eastern Arabian Sea. *Quarterly Journal of the Royal Meteorological Society*, *125*, 787–809. doi:[10.1002/qj.49712555503](https://doi.org/10.1002/qj.49712555503).

Raven, J. A. (1998). The twelfth Tansley lecture. Small is beautiful: the picophytoplankton. *Functional Ecology*, *12*, 503–513. doi:[10.1046/j.1365-2435.1998.00233.x](https://doi.org/10.1046/j.1365-2435.1998.00233.x).

Resplandy, L., Lévy, M., Bopp, L., Echevin, V., Pous, S., Sarma, V. V. S. S., & Kumar, D. (2012). Controlling factors of the oxygen balance in the Arabian Sea's OMZ. *Biogeosciences*, *9*, 5095–5109. doi:[10.5194/bg-9-5095-2012](https://doi.org/10.5194/bg-9-5095-2012).

Rochford, D. J. (1964). Salinity maxima in the upper 1000 m of the north Indian Ocean. *Australian Journal of Marine Freshwater Research*, *15*.

Sakamoto, C. M., Karl, D. M., Jannasch, H. W., Bidigare, R. R., Letelier, R. M., Waltz, P. M., Ryan, J. P., Polito, P. S., & S., J. K. (2004). Influence of Rossby waves on nutrient dynamics and the plankton community structure in the North Pacific subtropical gyre. *Journal of Geophysical Research*, *109*. doi:[10.1029/2003JC001976](https://doi.org/10.1029/2003JC001976).

Sarkar, K., Aparna, S. G., Dora, S., & Shankar, D. (2018). Seasonal variability of sea-surface temperature fronts associated with large marine ecosystems in the north Indian Ocean. *Journal of Earth System Science*, *128*, 20. URL: <https://doi.org/10.1007/s12040-018-1045-x>. doi:[10.1007/s12040-018-1045-x](https://doi.org/10.1007/s12040-018-1045-x).

Sarma, V. V. S. S. (2002). An evaluation of physical and biogeochemical processes regulating perennial suboxic conditions in the water column of the Arabian Sea. *Global Biogeochemical Cycles*, *16*, 29–1–29–11. doi:[10.1029/2001GB001461](https://doi.org/10.1029/2001GB001461).

Sarma, V. V. S. S. (2006). The influence of Indian Ocean Dipole (IOD) on biogeochemistry of carbon in the Arabian Sea during 1997–1998. *Journal of Earth System Science*, *115*, 433–450. doi:[10.1007/BF02702872](https://doi.org/10.1007/BF02702872).

Sasamal, S. K. (2006). Island mass effect around the Maldives during the winter months of 2003 and 2004. *International Journal of Remote Sensing*, *27*, 5087–5093. doi:[10.1080/01431160500177562](https://doi.org/10.1080/01431160500177562).

Schott, F. A., & McCreary, J. P. (2001). The monsoon circulation of the Indian Ocean. *Progress in Oceanography*, *51*, 1–123. doi:[10.1016/S0079-6611\(01\)00083-0](https://doi.org/10.1016/S0079-6611(01)00083-0).

Shankar, D., Gopalakrishna, V. V., Shenoi, S. S. C., Durand, F., S. R. Shetye, C. K. R., Johnson, Z., Araligidat, N., & Michael, G. S. (2004). Observational evidence for westward propagation of temperature inversions in the southeastern Arabian Sea. *Geophysical Research Letters*, *31*, L08305. doi:[10.1029/2004GL019652](https://doi.org/10.1029/2004GL019652).

Shankar, D., McCreary, J. P., Han, W., & Shetye, S. R. (1996). Dynamics of the East India Coastal Current: 1. Analytic solutions forced by interior Ekman pumping and local alongshore winds. *Journal of Geophysical Research*, *101*, 13975–13991.

Shankar, D., Remya, R., Anil, A., & Vijith, V. (2019). Role of physical processes in determining the nature of fisheries in the eastern Arabian Sea. *Progress in Oceanography*, *172*, 124–158. doi:[10.1016/j.pocean.2018.11.006](https://doi.org/10.1016/j.pocean.2018.11.006).

Shankar, D., Remya, R., Vinayachandran, P. N., Chatterjee, A., & Behera, A. (2016). Inhibition of mixed-layer deepening during winter in the northeastern Arabian Sea by the West India Coastal Current. *Climate Dynamics*, *47*, 1049–1072. doi:[10.1007/s00382-015-2888-3](https://doi.org/10.1007/s00382-015-2888-3).

Shankar, D., Shenoi, S. S. C., Nayak, R. K., Vinayachandran, P. N., Nampoothiri, G., Almeida, A. M., Michael, G. S., Kumar, M. R. R., Sundar, D., & Sreejith, O. P. (2005). Hydrography of the eastern Arabian Sea during summer monsoon 2002. *Journal of Earth System Science*, *114*, 459–474. doi:[10.1007/BF02702023](https://doi.org/10.1007/BF02702023).

Shankar, D., & Shetye, S. R. (1997). On the dynamics of the Lakshadweep high and low in the southeastern Arabian Sea. *Journal of Geophysical Research*, *102*, 12551–12562. doi:[10.1029/97JC00465](https://doi.org/10.1029/97JC00465).

Shankar, D., Vinayachandran, P., & Unnikrishnan, A. (2002). The monsoon currents in the north Indian Ocean. *Progress in Oceanography*, *52*, 63 – 120. doi:[10.1016/S0079-6611\(02\)00024-1](https://doi.org/10.1016/S0079-6611(02)00024-1).

Shenoi, S. S. C., Shankar, D., Michael, G. S., Kurian, J., Varma, K. K., Kumar, M. R. R., Almeida, A. M., Unnikrishnan, A. S., Fernandes, W., Barreto, N., Gnanaseelan, C., Mathew, R., Praju, K. V., & Mahale, V. (2005). Hydrography and water masses in the southeastern Arabian Sea during March–June 2003. *Journal of Earth System Science*, *114*, 475–491. doi:[10.1007/BF02702024](https://doi.org/10.1007/BF02702024).

Shenoi, S. S. C., Shankar, D., & Shetye, S. R. (1999). On the sea surface temperature high in the Lakshadweep Sea before the onset of the southwest monsoon. *Journal of Geophysical Research: Oceans*, *104*, 15703–15712. doi:[10.1029/1998JC900080](https://doi.org/10.1029/1998JC900080).

Shenoy, D. M., Suresh, I., Uskaikar, H., Kurian, S., Vidya, P., Shirodkar, G., Gauns, M. U., & Naqvi, S. (2020). Variability of dissolved oxygen in the arabian sea oxygen minimum zone and its driving mechanisms. *Journal of Marine Systems*, (p. 103310). doi:<https://doi.org/10.1016/j.jmarsys.2020.103310>.

Siegel, D. A. (2001). The Rossby rototiller. *Nature*, *409*, 576–577.

Suresh, I., Vialard, J., Izumo, T., Lengaigne, M., Han, W., McCreary, J., & Muraleedharan, P. M. (2016). Dominant role of winds near Sri Lanka in driving seasonal sea level variations along the west coast of India. *Geophysical Research Letters*, *43*, 7028–7035. doi:[10.1002/2016GL069976](https://doi.org/10.1002/2016GL069976).

Swallow, J. (1984). Some aspects of the physical oceanography of the Indian Ocean. *Deep Sea Research Part A. Oceanographic Research Papers*, *31*, 639–650. doi:[10.1016/0198-0149\(84\)90032-3](https://doi.org/10.1016/0198-0149(84)90032-3).

Thushara, V., & Vinayachandran, P. N. (2016). Formation of summer phytoplankton bloom in the northwestern Bay of Bengal in a coupled physical-ecosystem model. *Journal of Geophysical Research*, *121*, 8535–8550. doi:[10.1002/2016JC011987](https://doi.org/10.1002/2016JC011987).

Thushara, V., & Vinayachandran, P. N. (2020). Unprecedented surface chlorophyll blooms in the southeastern Arabian Sea during an extreme negative Indian Ocean Dipole. Submitted.

Thushara, V., Vinayachandran, P. N. M., Matthews, A. J., Webber, B. G. M., & Queste, B. Y. (2019). Vertical distribution of chlorophyll in dynamically distinct regions of the southern Bay of Bengal. *Biogeosciences*, *16*, 1447–1468. doi:[10.5194/bg-16-1447-2019](https://doi.org/10.5194/bg-16-1447-2019).

Uz, B. M., Yoder, J. A., & Osychny, V. (2001). Pumping of nutrients to ocean surface waters by the action of propagating planetary waves. *Nature*, *409*, 597–600. doi:[10.1038/35054527](https://doi.org/10.1038/35054527).

Vijith, V., Vinayachandran, P. N., Thushara, V., Amol, P., Shankar, D., & Anil, A. C. (2016). Consequences of inhibition of mixed-layer deepening by the West India Coastal Current for winter phytoplankton bloom in the northeastern Arabian Sea. *Journal of Geophysical Research*, *121*. doi:[10.1002/2016JC012004](https://doi.org/10.1002/2016JC012004).

Vinayachandran, P. N., Chauhan, P., Mohan, M., & Nayak, S. (2004). Biological response of the sea around Sri Lanka to summer monsoon. *Geophysical Research Letters*, *31*. doi:[10.1029/2003GL018533](https://doi.org/10.1029/2003GL018533).

Vinayachandran, P. N., Neema, C. P., Mathew, S., & Remya, R. (2012). Mechanisms of summer intraseasonal sea surface temperature oscillations in the Bay of Bengal. *Journal of Geophysical Research: Oceans*, *117*. doi:[10.1029/2011JC007433](https://doi.org/10.1029/2011JC007433).

de Vos, A., Pattiaratchi, C. B., & Wijeratne, E. M. S. (2014). Surface circulation and upwelling patterns around Sri Lanka. *Biogeosciences*, *11*, 5909–5930. doi:[10.5194/bg-11-5909-2014](https://doi.org/10.5194/bg-11-5909-2014).

Ward, B., Olson, R. J., & Perry, M. J. (1982). Microbial nitrification rates in the primary nitrite maximum off southern California. *Deep Sea Research Part A. Oceanographic Research Papers*, *29*, 247–255. doi:[10.1016/0198-0149\(82\)90112-1](https://doi.org/10.1016/0198-0149(82)90112-1).

White, W. B., Gloersen, K. A., Marsac, F., & Tourre, Y. M. (2004). Influence of coupled Rossby waves on primary productivity and tuna abundance in the Indian Ocean. *Journal of Oceanography*, *60*, 531–541.

Wiggert, J., Jones, B., Dickey, T., R.A., W., Brink, K., J., M., & Codispoti, L. (2000). The northeast monsoons impact on mixing, phytoplankton biomass and nutrient cycling in the Arabian Sea. *Deep-Sea Research II*, *47*, 1353-1385.

Wiggert, J., Murtugudde, R., & McClain, C. (2002). Processes controlling interannual variations in wintertime (Northeast Monsoon) primary productivity in the central Arabian Sea. *Deep Sea Research Part II: Topical Studies in Oceanography*, *49*, 2319–2343. doi:[10.1016/S0967-0645\(02\)00039-5](https://doi.org/10.1016/S0967-0645(02)00039-5). The 1994-1996 Arabian Sea Expedition: Oceanic Response to Monsoon al Forcing, Part 5.

Young, D. K., & Kindle, J. C. (1994). Physical processes affecting availability of dissolved silicate for diatom production in the Arabian Sea. *Journal of Geophysical Research: Oceans*, *99*, 22619–22632. doi:[10.1029/94JC01449](https://doi.org/10.1029/94JC01449).

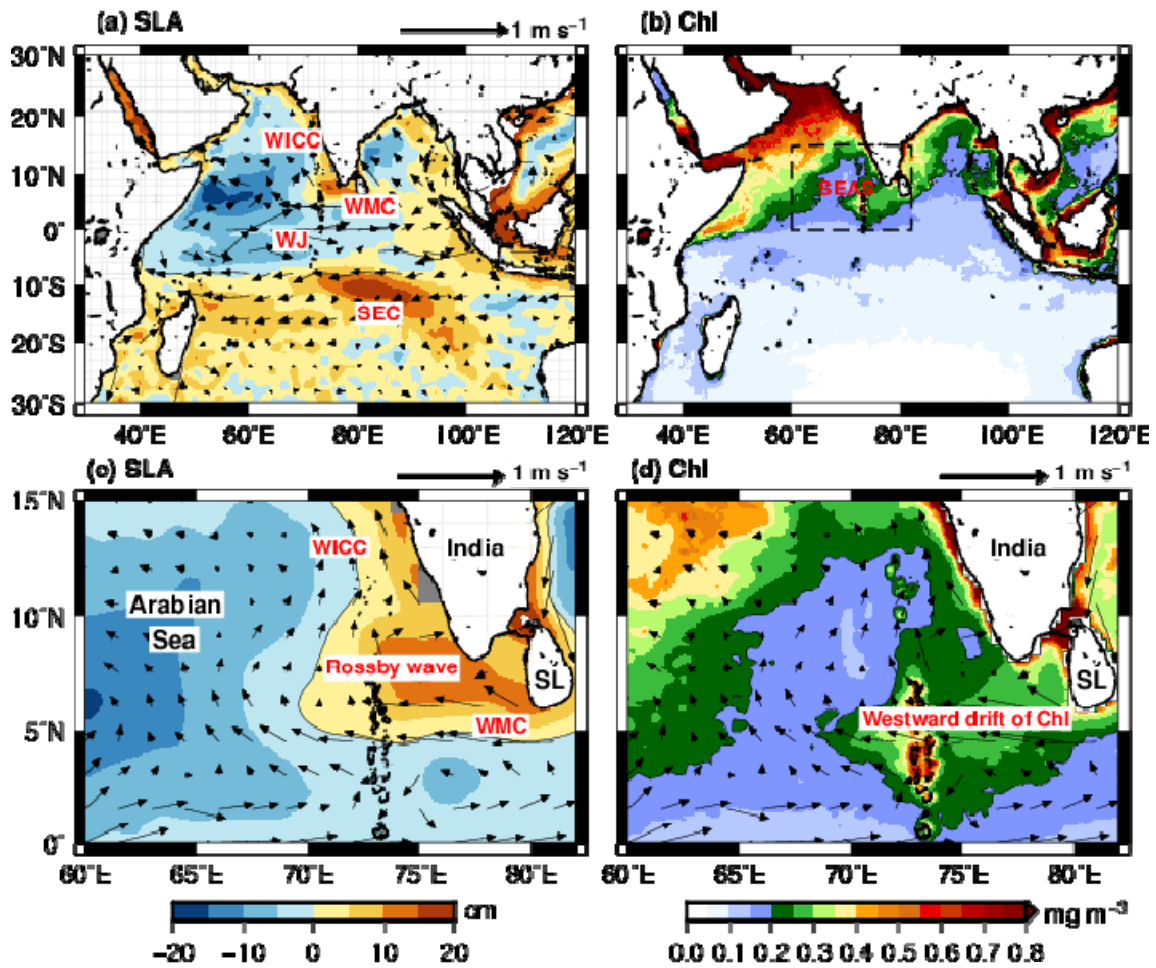


Figure 1: December climatology of (a) sea level anomaly and (b) chlorophyll for the Indian Ocean. The dashed box in (b) is the region of interest. (c)–(d) Same as panels (a) and (b) but for the SEAS (region of interest). The panels highlight the westward drift of Rossby wave and surface chlorophyll in the SEAS during the winter monsoon. The vectors shown are surface currents from OSCAR. Abbreviations in panel (a) and (c) are WICC, West India Coastal Current; WMC, Winter Monsoon Current; WJ, Wyrтки Jet; SEC, South Equatorial Current; SEAS, Southeastern Arabian Sea, SL, Sri Lanka. The contours represents zero sea level in (a) and (c) and 0.2 mg m^{-3} in (b) and (d).

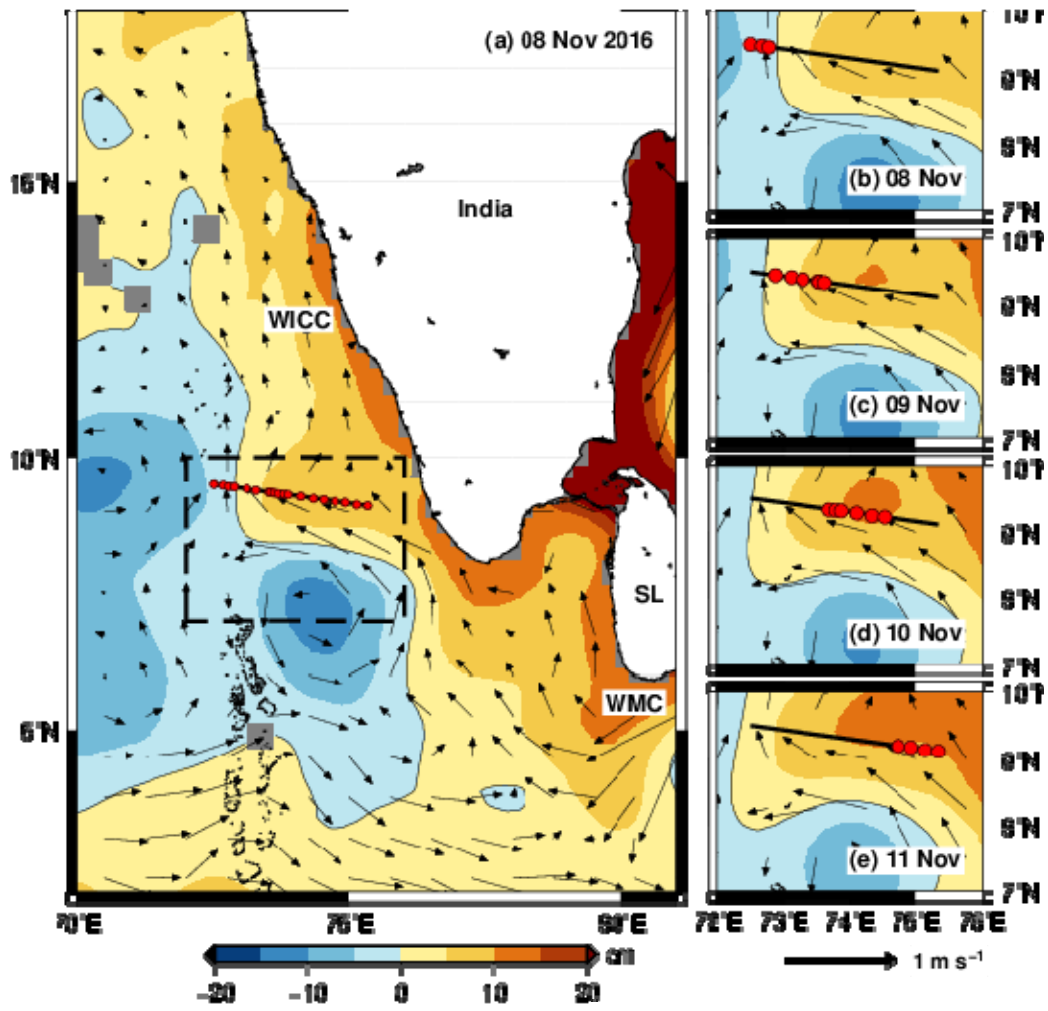


Figure 2: (a) Figure showing a hydrographic transect across the Rossby front from 08–11 November 2016. In the background, the OSCAR current vectors (m s^{-1}) are overlaid over sea level (cm). The red dots are the stations, and the contour is zero sea level. The panels (b)–(e) on the right show the westward propagation of Rossby wave during the sampling period. By the time the last station has been sampled, the wave has already crossed the first station.

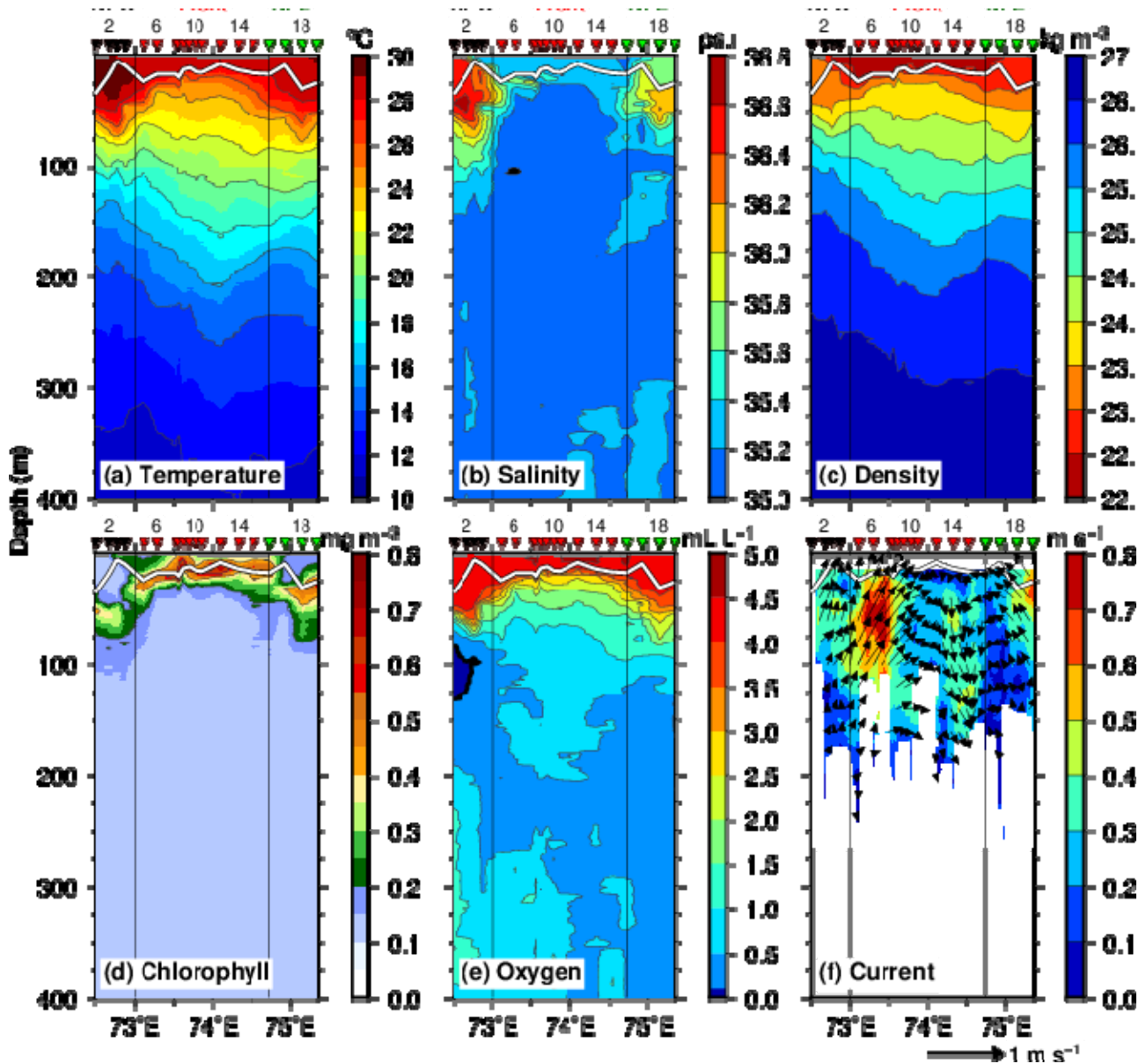


Figure 3: Hydrographic observations from the transect shown in Figure 2. The small inverted triangles mark the stations. The first and last four stations represent the non-front west (NFW) and non-front east stations (NFE), respectively. The remaining stations in the middle are the frontal stations. Selected stations are numbered above the inverted triangles for reference. The thick white contour shows the mixed-layer depth. The dark-blue region in (e) highlights the suboxic condition ($0 < O_2 < 0.1 \text{ mL L}^{-1}$). The region lies roughly between 90–115 m in NFW. The currents in (f) are from 150 kHz vessel-mounted ADCP. Both the magnitude ($\sqrt{u^2 + v^2}$) and vectors show the horizontal velocities with depth. For example, the arrows pointing right (up) represent the eastward (northward) flow. The vertical component is not used for the computation of the magnitude or direction of the current.

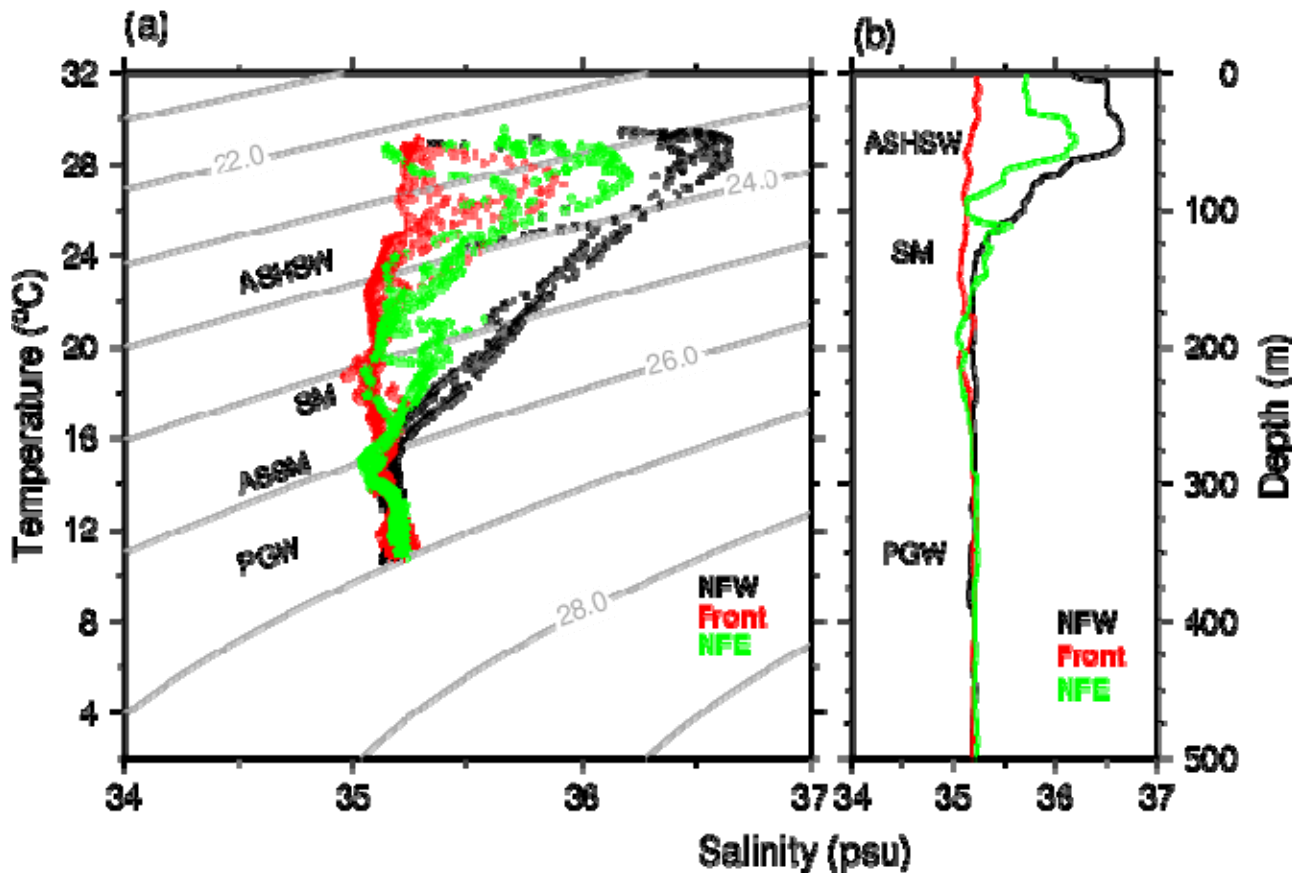


Figure 4: (a) Temperature-salinity (TS) diagram for NFE (black), Front (red), and NFW (green). The contours are of σ_t (kg m^{-3}). Salinity profiles picked from NFW (Station 2), Front (Station 14), and NFE (Station 18) (see Figure 3 for station numbers). The abbreviations in panels (a) and (b) are ASHSW, Arabian Sea High Salinity Water; PGW, Persian Gulf Water; ASSM, Arabian Sea Salinity Minimum; SM; Secondary Maximum.

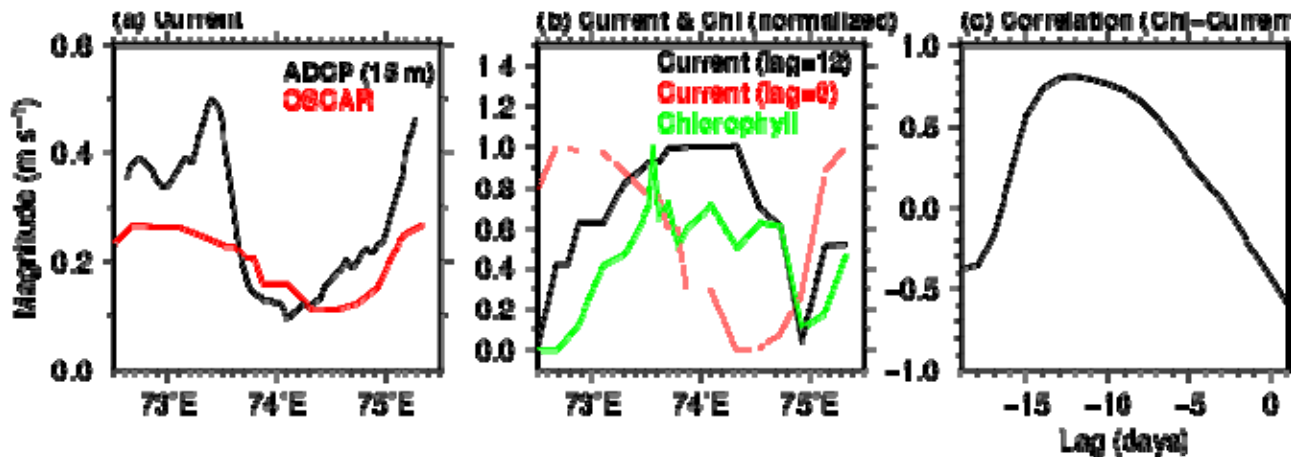


Figure 5: (a) OSCAR and ADCP currents at 15 m along the cruise track. A 0.25° box-car filter was used to smooth the ADCP current. (b) Comparison between near-surface chlorophyll from fluorometer and OSCAR current along the track. The currents are shown at 12-day (black) and zero-day (red) lag. All the values are normalised for comparison, and the chlorophyll is averaged over the top 30 m. (c) Spatial cross-correlation between chlorophyll and OSCAR current. For lag computation, the currents from OSCAR are picked along the track for each day before the sampling the time. For example, a 12-day lag means that the current leads the chlorophyll by 12 days at the sampling station.

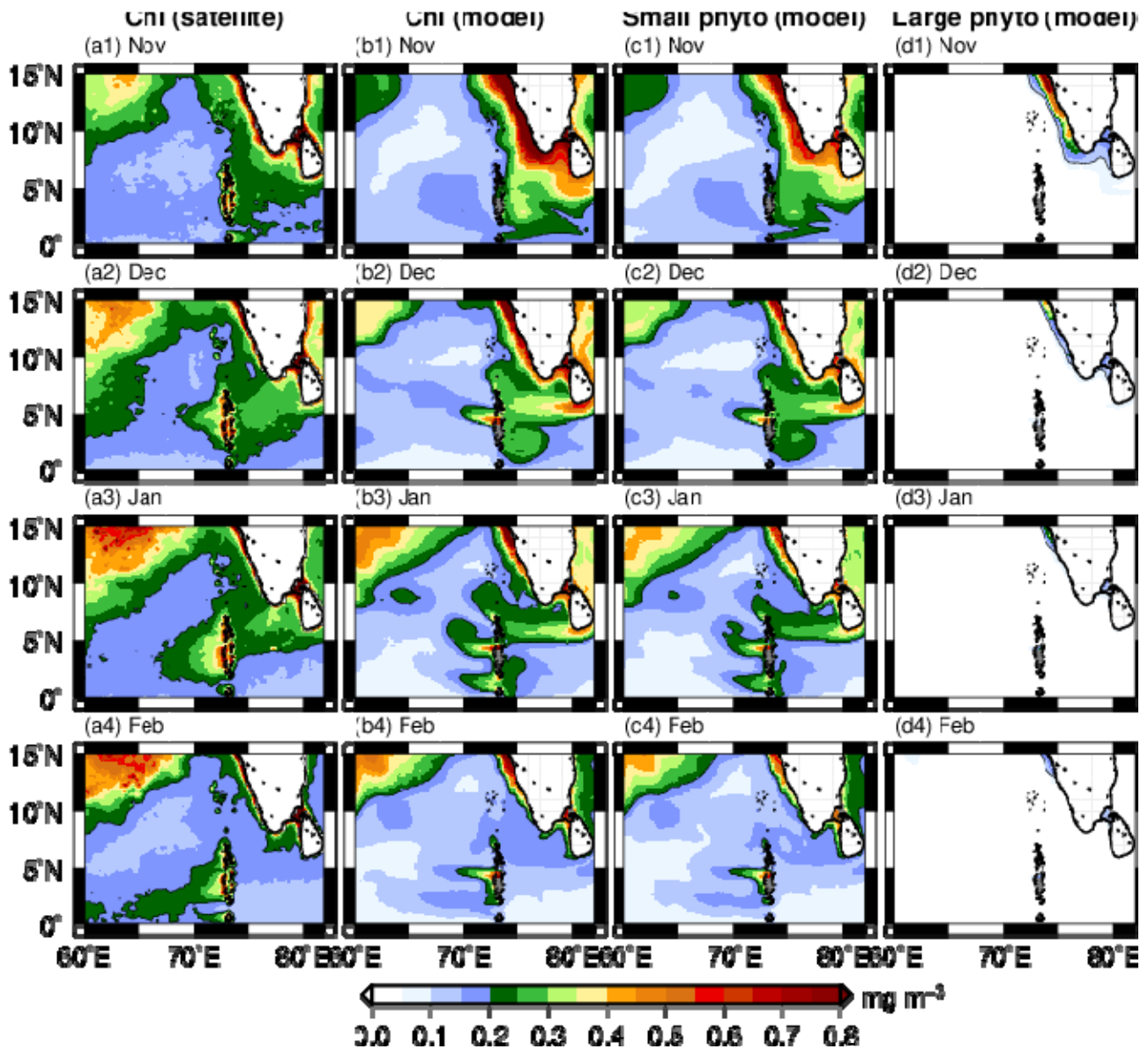


Figure 6: Comparison of monthly climatology of surface chlorophyll between SeaWiFS (a1)–(a4) and model (b1)–(b4). Chlorophyll based on phytoplankton functional groups from the model for (c1)–(c4) small phytoplankton and (d1)–(d4) large phytoplankton. The model chlorophyll is averaged over the top 30 m.

Figure 6: Comparison of monthly climatology of surface chlorophyll between SeaWiFS (a1)–(a4) and model (b1)–(b4). Chlorophyll based on phytoplankton functional groups from the model for (c1)–(c4) small phytoplankton and (d1)–(d4) large phytoplankton. The model chlorophyll is averaged over the top 30 m.

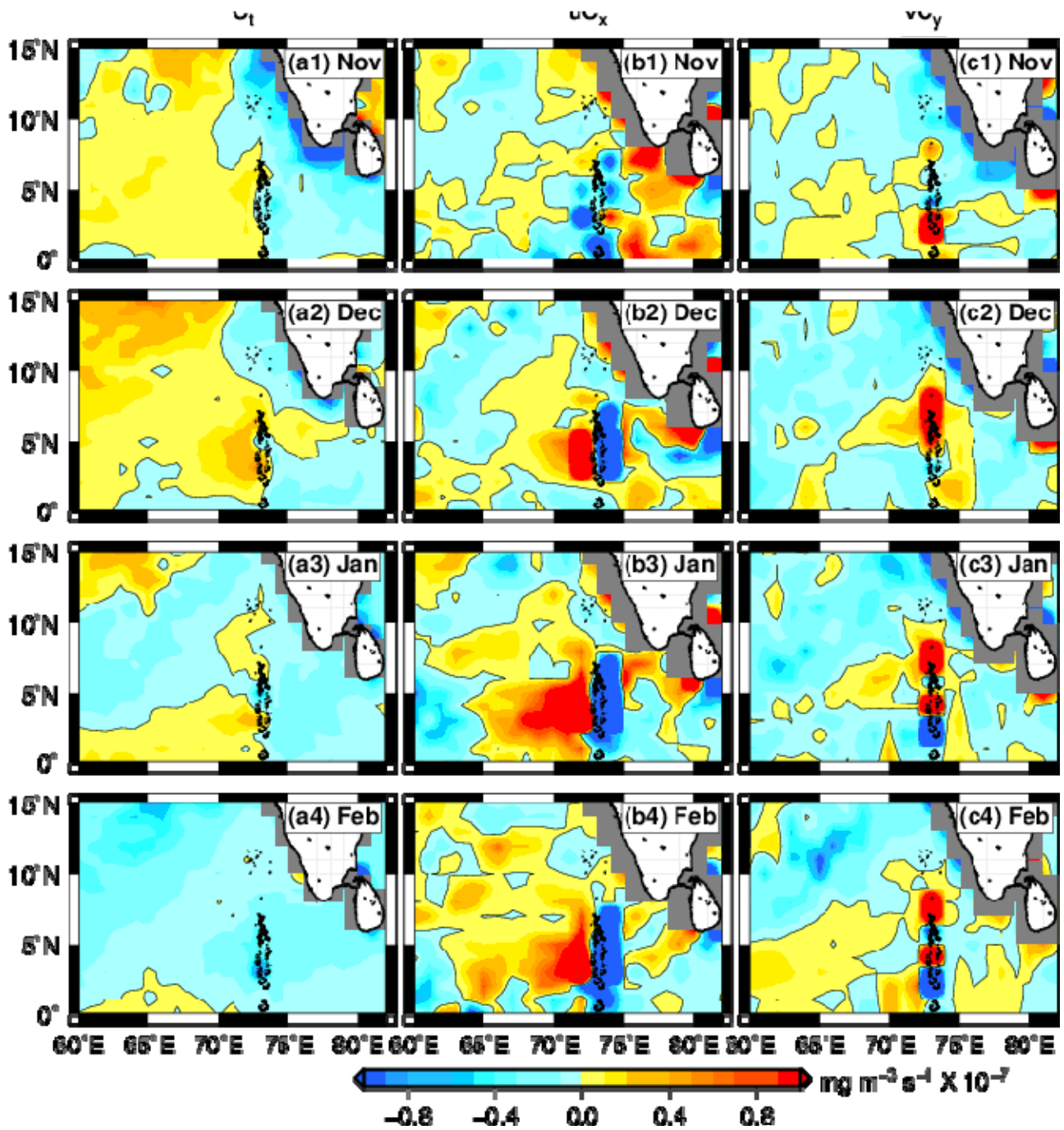


Figure 7: Budget terms computed using climatology of satellite chlorophyll data: (a1)–(a4) tendency, (b1)–(b4) zonal advection, and (c1)–(c4) meridional advection terms. The monthly climatology was regridded to $1^\circ \times 1^\circ$ before computing the derivatives using the centred difference scheme.

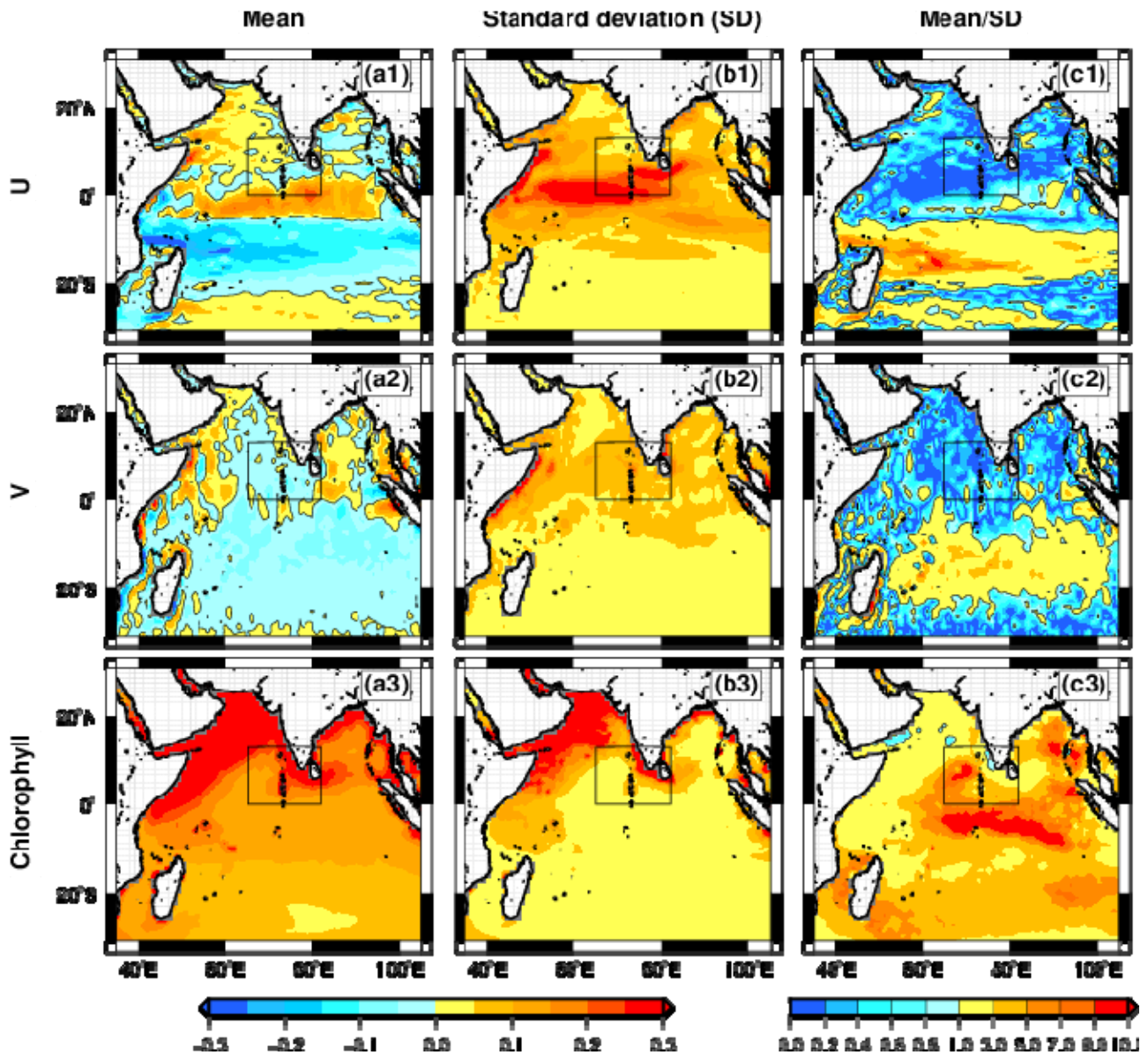


Figure 8: Figure showing the mean, standard deviation, and their ratio for OSCAR currents (m s^{-1}) and chlorophyll (mg m^{-3}). The red colour in the third panel (c1–c3) indicates that the mean is greater than the standard deviation, and the blue colour indicates that the standard deviation is greater than the mean. Here, the word ‘mean’ also implies mean annual climatology. The standard deviation is computed using monthly climatology, and the absolute mean is used to compute the ratio. The box marks the region of interest or the SEAS.

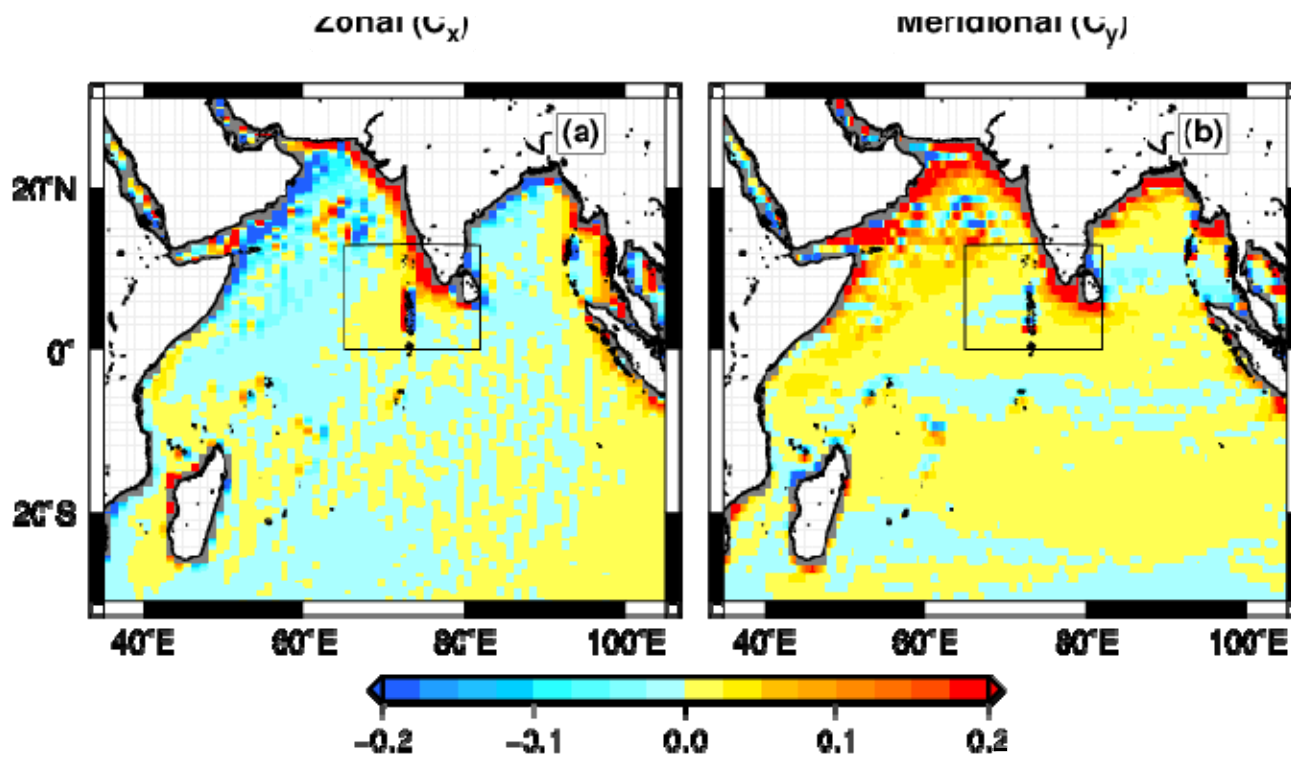


Figure 9: The annual mean chlorophyll gradient ($\text{mg m}^{-3} \text{ degree}^{-1}$) calculated from SeaWiFS for the Indian Ocean. The left panel shows the zonal gradient, and the right panel shows the meridional gradient. The box marks the region of interest or the SEAS.

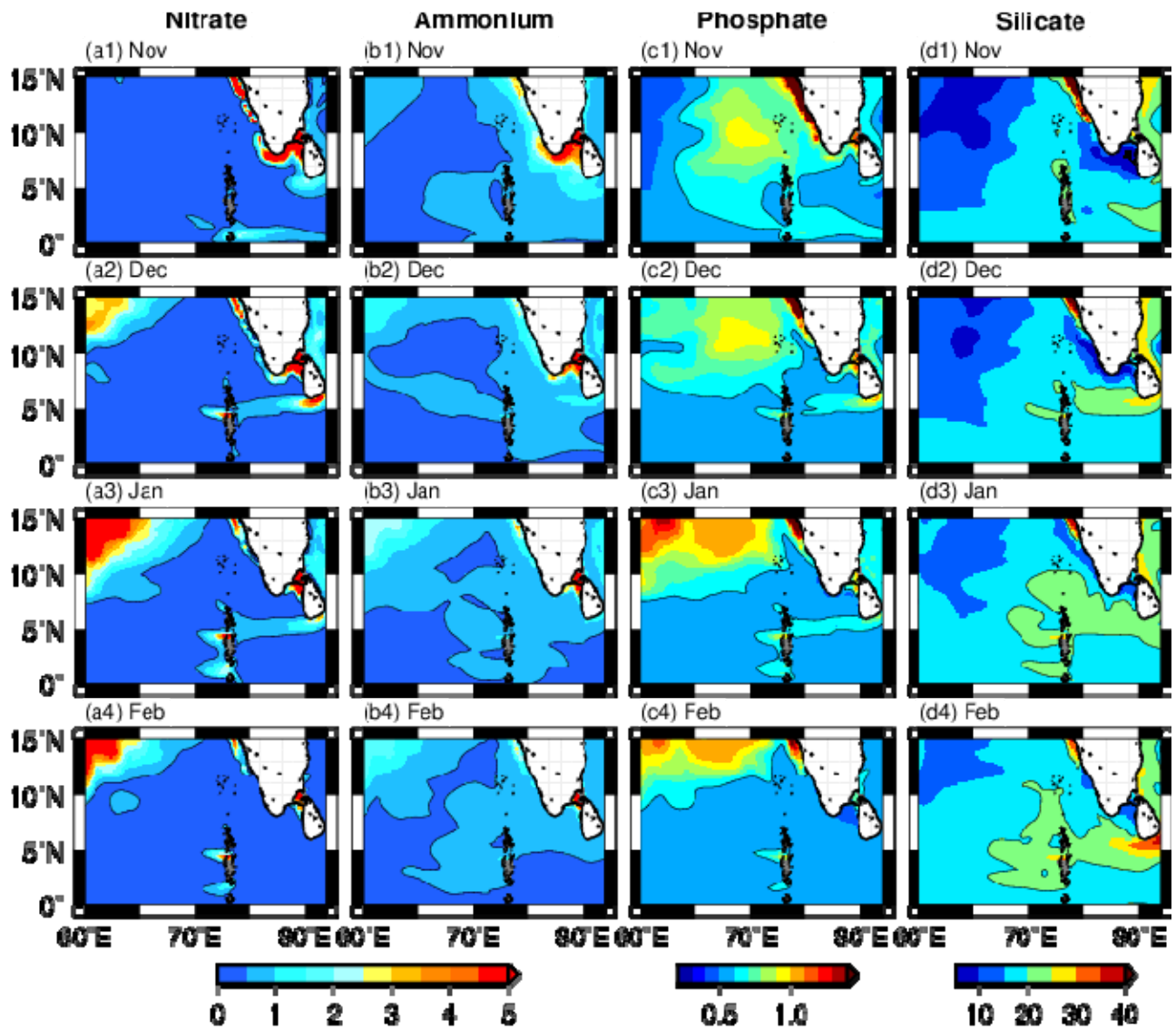


Figure 10: Monthly climatology of (a1)–(a4) nitrate, (b1)–(b4) ammonium, (c1)–(c4) phosphate, and (d1)–(d4) silicate from the model. The units are in $\mu\text{mol kg}^{-1}$.

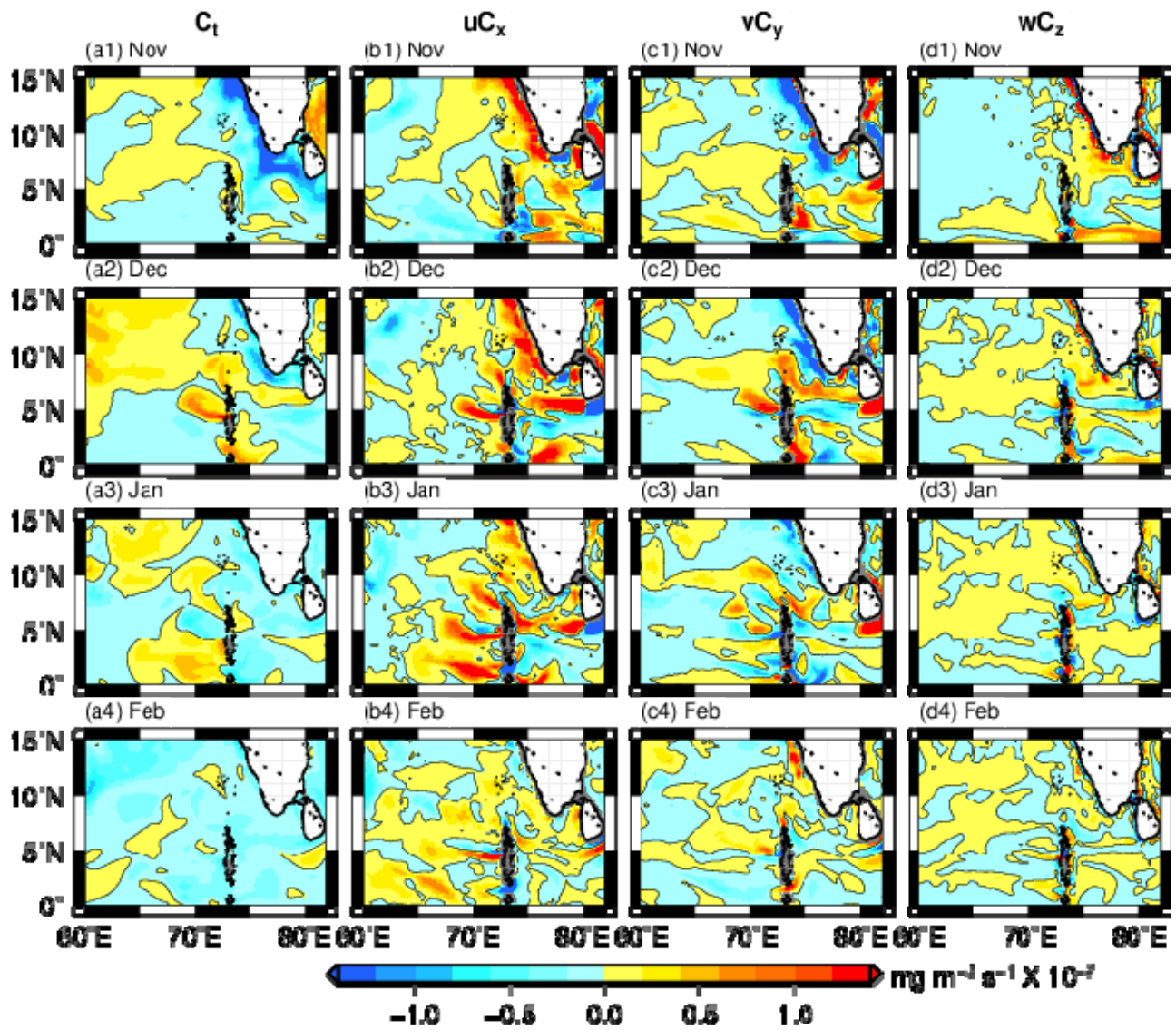


Figure 11: Monthly averaged budget terms computed using model chlorophyll data: (a1)–(a4) tendency term, (b1)–(b4) zonal advection, and (c1)–(c4) meridional advection, and (d1)–(d4) vertical advection terms.

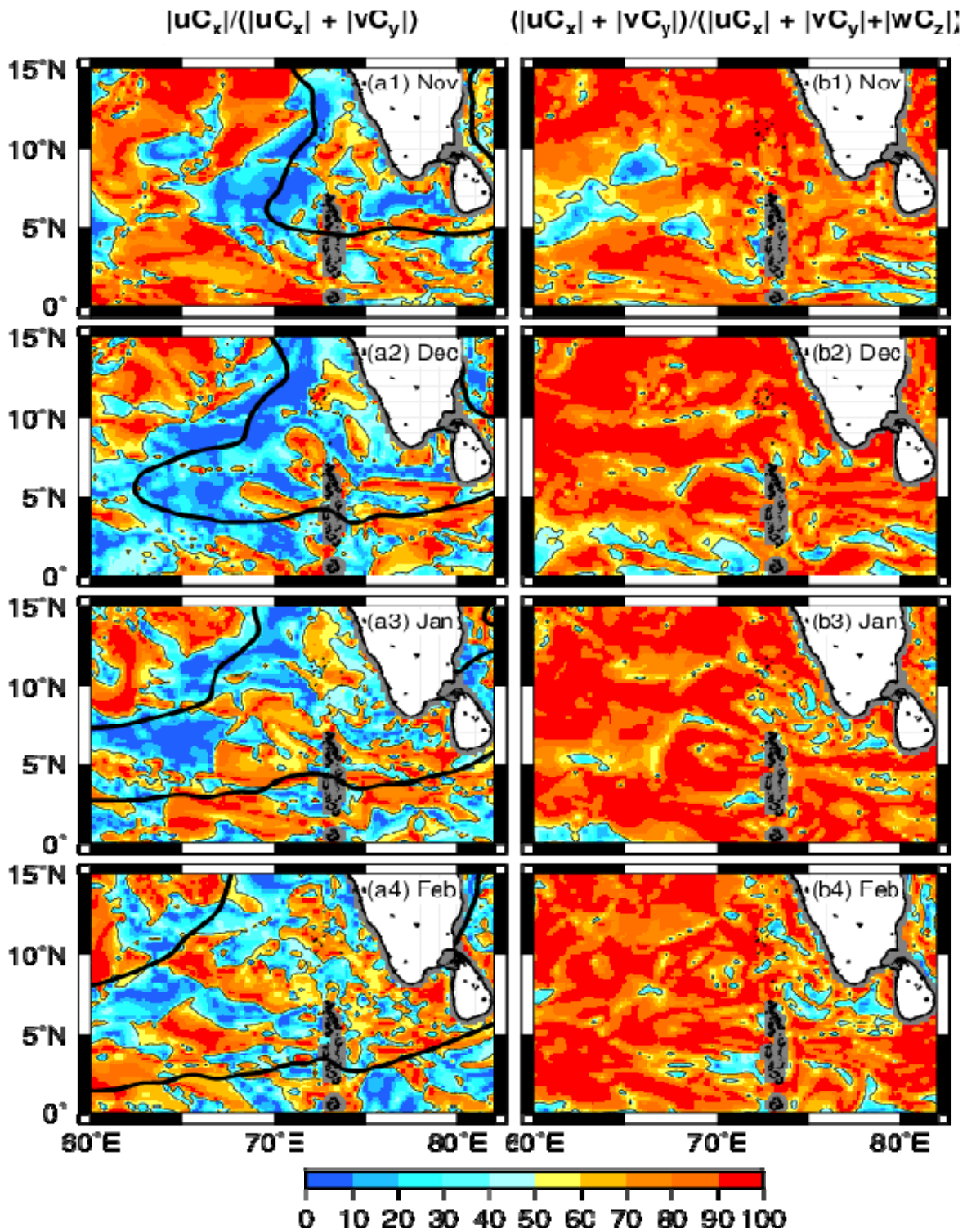


Figure 12: (a1–a4) The ratio of zonal advection to horizontal advection in percentage. Absolute values are used for computing the ratios. Blue (red) colour implies meridional (zonal) advection is strong. The thin contour is 50%, and the thick contour is zero sea level from satellite climatology for the following month. (b1–b4) The ratio of horizontal advection to total advection. Blue (red) colour implies vertical advection (horizontal) is strong.

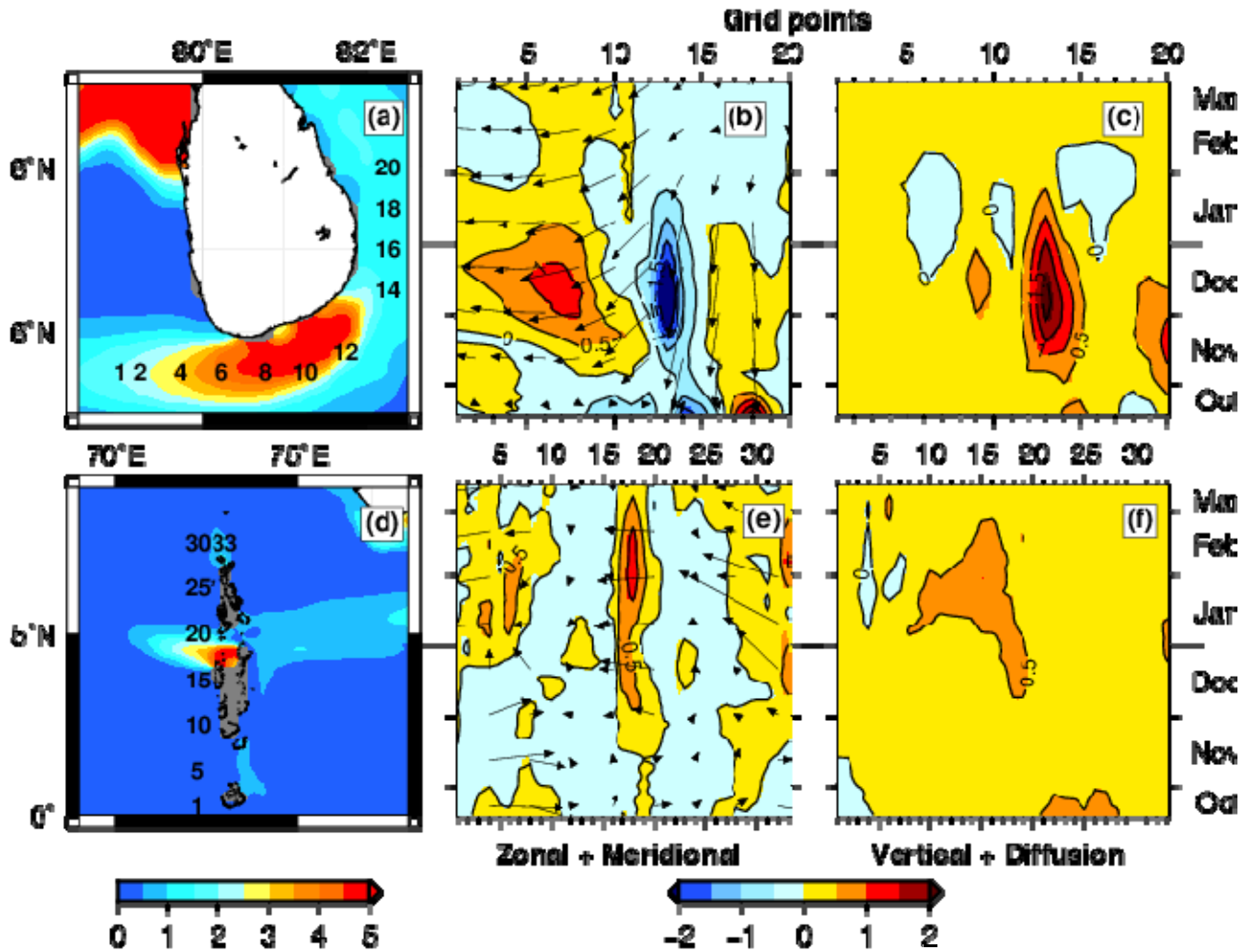


Figure 13: (a) December climatology of nitrate from the model shown for the region around Sri Lanka. The numbers show the grid points where the nitrate budget is computed. (b) Sum of zonal and meridional advection shown for the grid points from panel (a) from October to March. (c) Sum of vertical advection and diffusion. (d)–(f) Same as panels (a)–(c) but for the region around the Maldives.